ELECTRON SPIN RESONANCE BASED INVESTIGATIONS OF COPPER DOPED ZEOLITES AS

SELECTIVE CATALYTIC REDUCTION CATALYSTS FOR deNOx APPLICATIONS

by

VIRAL SAGAR

a thesis submitted to the

Graduate School New Brunswick

Rutgers, The State University of New Jersey

in partial fulfillment of the requirements

for the degree of

Master of Science

Graduate program in Chemical and Biochemical Engineering

written under the direction of

Professor Gerard Charles Dismukes

and approved by

_____

_____

_____

New Brunswick, New Jersey

October 2015

ABSTRACT OF THE THESIS

Electron Spin Resonance based investigations of Copper doped Zeolites as Selective

Catalytic Reduction catalysts for deNOx applications

by VIRAL SAGAR

Thesis Director:

Professor Gerard Charles Dismukes

 Electron spin resonance (ESR) is an excellent spectroscopic tool to detect speciation transitions in paramagnetic samples. This research studies the activity of copper doped zeolite catalysts that breakdown the atmospheric pollutant NOx gases in diesel engine exhaust emissions. Copper exhibits +1, +2, +3 and +4 oxidation states with $3d^9$ as outer shell electronic configuration for +2 oxidation state, which is most favored and detectable with Electron Spin Resonance (ESR) spectroscopy. Copper exhibits multiple coordinations such as tetra-, penta-, hexa- or octa- coordinate forms out of which four coordinate or tetra forms are preferred in the +2 state. The determination of this geometry, which affects electronic properties of Cu^{2+} ions, is important to know the ground state of a certain arrangement through the order of energy levels of d orbital. The electronic g factor with the copper nuclear hyperfine splitting can be indicators of the geometry and the nature of spatial distribution of unpaired spin orbital of the

copper center in zeolite as SCR catalysts. Our focus is on elucidating the mechanism at the metal center microenvironment that causes the catalytic activity. This research will drive the improvement in the molecular design of these catalysts and hence help advance environmental chemistry approach in reduction of atmospheric pollution from NO_x gas emissions.

Acknowledgement

Then, I would like to express my sincere thankfulness to Professor Gerard Charles Dismukes for trusting in me with this research project. His continuous guidance and thorough tutelage were tremendously helpful in accomplishing the milestones of this project. His diverse expertise helped probe the research problem better.

Next, I would like to thank the Dismukes Lab catalysis & biosolar research group members for their helpfulness and patience with my naive questions, constructive discussions and jovial chats at random times.

Further, I would like to thank Alexei Tyrishkin (Princeton University) for the training provided for liquid helium ESR measurements.

Also, I would like to thank departmental staff of Chemistry & Chemical Biology and Chemical & Biochemical Engineering for their support with routine procedures, laboratory set up and maintenance. I would specifically like to mention Alexei Ermakov, for his help with the electrical aspect of instrumentation and John Furnari, for his help with the computers.

Lastly, I would like to thank my parents, family, friends and Rutgers colleagues for their support, motivation and time they spent on me.

Dedicated to

… my mother Mrs Geeta Haresh Sagar, family, Professor Dismukes, readers and the world at large for the advancement of science.

Table of contents

List of tables

List of illustrations

List of specific abbreviations

*BEA – Beta polymorph A zeolite

1D – One Dimensional

a – Hyperfine splitting (mT or G)

A – Hyperfine coupling constant (cm^{-1})

B – Magnetic field strength (mT or G)

CHA – Chabazite

CW – Continuous Wave

ESR – Electron Spin Resonance

FAU – Faujasite

g – g factor = g_e (1-σ)

H_2O – water/aqua as a ligand

LHe – liquid helium

LN2 – liquid nitrogen

MOR – Mordenite

NOx – nitric oxide (NO) and nitrogen dioxide (NO_2)

SCR – Selective Catalytic Reduction

Si/Al – silicon/aluminum ratio of zeolite

SOx – sulfur oxides such as SO, SO_2, SO_3, SO_4, S_2O and S_2O_2

ZSM – Zeolite Socony Mobil

μ_B = Bohr magneton

1. Introduction

1.1 Selective Catalytic Reduction with zeolites

Selective Catalytic Reduction (SCR) is the process of reducing toxic pollutant NO_x gases to elemental N_2 and H_2O that are safely eliminated with the help of catalysts. Additionally, a modification of this technique for breaking complex molecules into commercially important products in fluid catalytic cracking is also used industrially [1]. Almost all SCR catalysts consist of a transition metal active site in small amounts supported on a bulk, a highly porous substrate such as zeolites. SCR in presence of ammonia (NH_3) is known to reduce the dangerous NO_x gases to elemental N_2 since the 1950's [2], with first commercial application in 1978 by IHI corporation [3]. The early research work using zeolites had Y type structure from faujasite family, with copper present as active component from transition metal series [4]. Since then the field has seen tremendous research and development on SCR catalysts. The early commercial catalysts involved vanadium based catalysts that were widely used for stationary optimal temperature performance but such catalysts suffered from low hydrothermal stability at extreme temperatures for advanced applications. Since then, multiple candidates proposed as exhibiting considerable stability under certain conditions were reported but only few seem to withstand the extreme temperature fluctuations that these catalysts are required to undergo. SCR for reducing NO_x gases is applied in stationary as well as mobile applications in petroleum fuel based engines. Currently,

bulk of the research efforts focus on mobile applications as it involves a wide range of extreme temperatures during normal operation under which the catalyst should perform optimally. Aqueous ammonia ($NH_{3, aq}$) or urea ($CO(NH_2)_2$) is used in SCR to aid in the redox reactions as a reductant. The typical diesel exhaust gas temperatures could range from 150 – 1000 °C with catalytic activity operational in the window of 150 – 850 °C. Diesel engines are known for their higher efficiency in operation due to high energy value and low cost of diesel, but using diesel as a fuel involves emission of several pollutants such as NO_x and SO_x gases. The early commercial vanadium based catalysts used in catalytic cracking would mostly start decomposing when subjected to temperatures exceeding 550 °C with emission of vanadium that is toxic under emission standards. This led to extensive research and development in finding alternative stable catalysts for application in SCR. The zeolites were sufficiently researched by then and were explored as possible candidates for catalysts. Zeolites of the ZSM, Faujasite (FAU), Chabazite (CHA), etc types were reported containing transition elements such as copper, iron, etc in literature [5, 6 and 7]. Early tests indicated that copper containing zeolite based catalysts outperformed other transition metal based catalysts for reducing NO_x gases to N_2 under reaction conditions [8, 9 and 10]. This led to specific interest in developing and characterizing many copper containing zeolites and understanding their stability with performance characteristics under extreme conditions. Next, we discuss some of the properties of zeolites used as framework for these catalysts.

1.2 Types of zeolites and their structures

Zeolites are a class of minerals found in nature as aluminosilicates, sometimes in defined stoichiometric ratios. Materials are classified as macroporous (having pore widths larger than 50 nm), mesoporous (having pore widths between 2 – 50 nm) and microporous (having pore widths less than 2 nm) [11]. Microporous materials, such as zeolites, are widely used industrially due to their several properties, most important being specific size control in SCR. Zeolites are further classified as mordenite (MOR), beta polymorph A (BEA), faujasite (FAU), chabazite (CHA), etc based on the fundamental framework involved and the stoichiometric ratio of elements involved. Zeolites commonly contain alkali metals, hydrogen, silica, alumina, water, etc as building blocks. Table 1 summarizes some of the commonly used zeolites in SCR catalysis with their structures and stoichiometric formulae. For the purposes of this research, we studied two types of zeolites specifically faujasite (FAU) of Y-type and chabazite (CHA) of SSZ-13 type.

Table 1. Common zeolites used in copper based SCR catalysts.
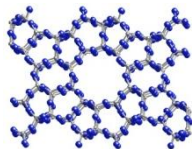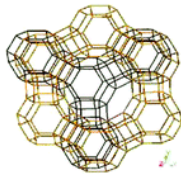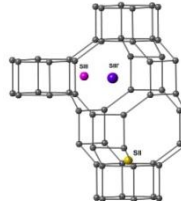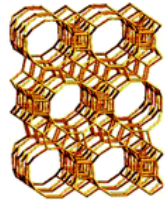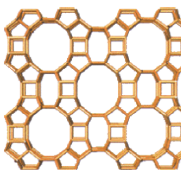
Name	Framework	Example	Chemical formula	Structure
ZSM-5	MFI	ZSM-5	$|Na^+_n (H_2O)_{16}|$ $[Al_nSi_{96-n} O_{192}]$ $n < 27$ [16]	[12]

Table 1. Common zeolites used in copper based SCR catalysts (continued).

Name	Framework	Example	Chemical formula	Structure
Faujasite	FAU	Y type	$\|(Ca^{2+},Mg^{2+}Na^{+}_2)_{29}\,(H_2O)_{240}\|$ $[Al_{58}Si_{134}\,O_{384}]$ [16]	[14]
Chabazite	CHA	SSZ-13	$\|Ca^{2+}_6\,(H_2O)_{40}\|\,[Al_{12}Si_{24}\,O_{72}]$ [16]	[18]
Beta polymorph A	*BEA	CIT-6	$\|Na^{+}_7\|\,[Al_7Si_{57}\,O_{128}]$ [16]	[14]
Mordenite	MOR	LZ-211	$\|Na^{+}_8\,(H_2O)_{24}\|\,[Al_8Si_{40}\,O_{96}]$ [16]	[20]

1.2.1 Faujasite

Faujasite is a type of zeolite found in nature containing different alkali metals such as sodium (Na), potassium (K) and/or magnesium (Mg). Due to irregularly defined pore channels and lack of proper stoichiometric compounds, most zeolites are commercially synthesized. They are predominantly distinguished as X type (Si/Al = 2-3) and Y type (Si/Al > 3) depending on Si/Al ratio with same molecular formula as in Table 1. The X type is predominantly used in catalytic cracking whereas the Y type has been applied in SCR catalysis. The Y type offers specific site based and structural advantages that are utilized in SCR catalysis. These site based advantages are offered from higher Si/Al ratio and structural advantages offered stability at higher temperatures, overall contributing to increased activity.

1.2.2 Chabazite

Chabazite is a type of zeolite found in nature, in sodium (Na) or hydrogen (H) form. It is one of the rare types of zeolite found in nature in almost purely stoichiometric ratio. It is synthesized commercially to suit specific structural needs. There are several types of chabazites such as SSZ-13, SAPO-34, etc [16], which are commercially synthesized for various applications. These vary depending on the Si/Al ratio and structure directing agent. For the purposes of this thesis, we explore the effects of calcination and hydrothermal treatment on SSZ-13 structural type of chabazite zeolites.

1.3 Metal doping effects

The first row elements of the d block or the transition metal group are most commonly used for catalysis due to their relative abundance and specific properties in reactions. For the purposes of SCR, most of the research has focused on copper (Cu) as dopant in zeolites with some work exploring iron (Fe) as another possible dopant. Such dopants when located at specific sites in the zeolite framework significantly increase the catalytic activity for NH_3 SCR in $deNO_x$ reactions. However, even in cases of irregular doping in zeolitic framework, in general, the copper doping significantly outperforms iron doping in NO_x conversion reactions [8, 9 and 10]. There are several reasons ascribed to this such as performance from the perspective of redox potentials, charge transfer and relative ease of changing oxidation states based on ligand field environment. One reason could be the specific stabilization of d orbitals that occurs in copper compared to iron based on ligand environment that allows relatively more energetically favorable interactions in e_g orbital subset of the d orbitals. Based on previous work and available evidence [21, 22, 23 and 24], we chose copper as a dopant for the preparation of samples for this research project.

1.4 Utilization of Electron Spin Resonance as an analytical tool

This study aims to understand the coordination sphere of copper for effective SCR catalysis. Copper is usually found as a stable coordination complex in +2 oxidation state.

The change from ground state electronic configuration of [Ar] $3d^{10}4s^1$ to +2 oxidation state electronic configuration of [Ar] $3d^9$ occurs via the loss of two electrons. The +2 oxidation state is a stable state for copper in a complex based on energy favorability. In +2 oxidation state, there lies an unpaired electron in one of the e_g orbital subset of the d orbitals. This unpaired electron has a spin angular momentum with s = ½ state that has a magnetic field and an electric field. The energy differences exhibited due to this unpaired electron are utilized in Electron Spin Resonance (ESR) spectroscopy to detect the specific environment around this spin. ESR spectroscopy is the most direct investigation tool available to detect the series of changes around this spin that is on the copper center, which contributes to SCR catalytic reactions. There are no other known alternative spectroscopic tools that could be utilized for this kind of direct evidence based investigation for the copper center. Hence, throughout this research project we extensively used ESR spectroscopy to characterize the nature of copper present in these catalysts.

2. Electron Spin Resonance

Electron Spin Resonance (ESR) is defined by IUPAC as, "the form of spectroscopy concerned with microwave induced transitions between magnetic energy levels of electrons having a net spin and orbital angular momentum" [25]. The materials that have an unpaired electron are ESR active and exhibit paramagnetism.

2.1 Theory of Electron Spin Resonance spectroscopy

In ESR, the different energy states arise from the interactions of unpaired electron spin angular momentum with the induced magnetic field to produce the Zeeman effect [26].

2.1.1 Fundamentals of electron spin

Every electron has a magnetic moment and a spin associated with it as per the spin quantum number, $s = \frac{1}{2}$ under quantum mechanical model. Due to a phenomenon called the Zeeman effect/Zeeman field splitting, when an electron in exposed to external magnetic field of sufficient strength, these spins on the electron align either in parallel (spin down, $s = -\frac{1}{2}$) or in anti-parallel (spin up, $s = \frac{1}{2}$) fashion to the applied magnetic field. This creates two states of energy and the difference between these states is measured by ESR spectroscopy.

2.1.2 Energy level diagram and energy states
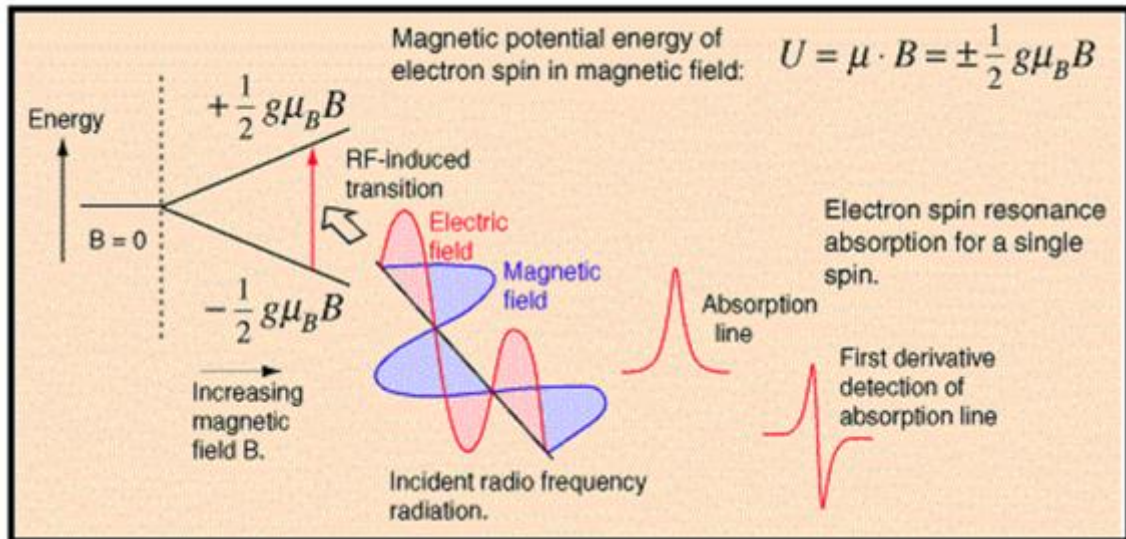
Figure 2.1. Energy level splitting diagram for single unpaired electron spin s=1/2 system such as hydrogen (H) [27].

The two energy states achieved by the electron spins on exposure to high magnetic fields are measured via resonance in ESR spectroscopy by applying incident microwaves of quantized energy 'hυ'. The excitation energy required to achieve resonance is given by the equation 1 below as described in figure 2.1,

$$h\upsilon = g\mu_B B = E_{1/2} - E_{-1/2} = \Delta E \qquad \text{equation 1}$$

here,   g = g factor = g_e (1-σ),

  μ_B = Bohr magneton and

  B = Magnetic field strength (mT or G).

This excitation energy is typically absorbed by the electron spins in the low energy state due to the Boltzmann distribution that allows the detection via the amount of energy absorbed from incident source by a paramagnetic sample. The Boltzmann distribution

law gives the ratio of the spins at higher level to that at lower level. At equilibrium, mathematically,

$$\frac{N_{upper}}{N_{lower}} = e^{\frac{-\Delta E}{k_b T}} = e^{-\frac{g\mu B}{k_b T}}$$

equation 2

where k_b is the Boltzmann constant.

Absorption condition is satisfied when the particles in lower state are higher than the particles in the higher state. This equation also implies that low temperature ESR spectroscopy is preferred to achieve higher resolution in energy splitting [28].

2.1.3 Description of fine structure, hyperfine structure and superhyperfine structure

In molecular systems, unpaired electrons are always delocalized over the molecular orbitals of atomic constituents to form stable complexes. This delocalization occurs via a change in angular momentum of the unpaired electrons, which due to relativistic effects causes shift in g factor from the unpaired electron g factor. In addition, the interactions of the electron spin with the non zero nuclear spin (I>0) will lead to a change in the lineshape of the ESR spectrum giving secondary peaks called hyperfine structure. Such changes yield significant information about the chemical structure of a system. A schematic indicating the difference between fine structure and hyperfine structure for hydrogen atom is shown in figure 2.2. Fine structure is typically 1000 times larger than hyperfine structure.

$$I = 1/2$$
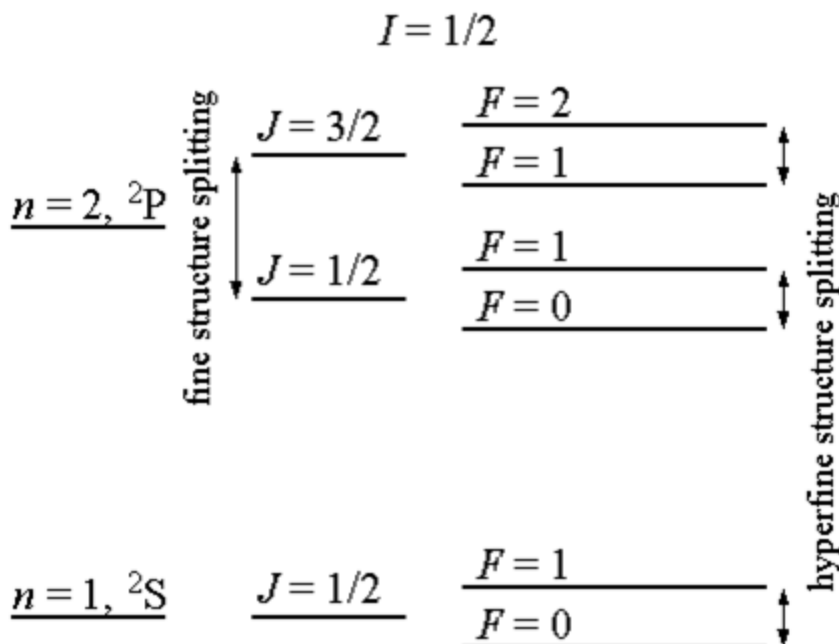
Figure 2.2. Distinction of resolution between fine structure and hyperfine structure in hydrogen atom (not drawn to scale) [29].

Superhyperfine splitting occurs when hyperfine splitting is split further due to unequal time spent by the unpaired electron on the independent nuclei involved in forming the complex. This superhyperfine splitting yields information about the bonding character of elements and significant insights in the ligand field picture of the complex [30].

2.1.4 Areas of application of ESR spectroscopy

ESR is a non destructive & highly focused tool for chemical analysis. Samples under study can be solids, liquids or gases. Multiple temperatures are utilized with prominent low temperature spectroscopy using liquid nitrogen and liquid helium as cooling media. Solid samples give either isotropic or anisotropic spectrum to yield information about

orientation dependence of paramagnetic centers in the external magnetic field. Many solid state materials and crystallites can be analyzed using ESR to understand the structural properties and charge mobility in the complex. Liquid samples with water have high dielectric constant and the sample will absorb most microwave power thereby hindering detection. A glassing agent can be used to reduce dielectric losses of water. Several biological metalloproteins, synthetic solutions, tissues, etc can be studied without tampering with physical characteristics of the sample. Gaseous samples are kept in sealed tubes, in near isothermal conditions for study.

Some broad uses of ESR spectroscopy are:

Detection of free radicals & ions in biological samples

Quantification of ESR active species

Geometry of the complex

Ligand bonding of the complex

Protein, biomolecules, biochemical analysis

Solid state physics

Quantum level analysis

Medicinal applications

Materials research

Biological studies

2.2 Experimental ESR spectroscopy

A typical spectrometer involves a source of light, a waveguide for light source, a carrier for light source in which the sample under study is kept, a reflector and a detector to record the energy changes that occurred to the incident light source. In ESR spectroscopy, a microwave power source such as a steady state diode, typically in X band (~9.5 GHz) frequency range is used with a waveguide and a resonator, usually a metal box that holds the sample. The detection occurs through reflection in the waveguide that is sent to a detector. The general block diagram of an ESR spectrometer is shown in figure 2.3.
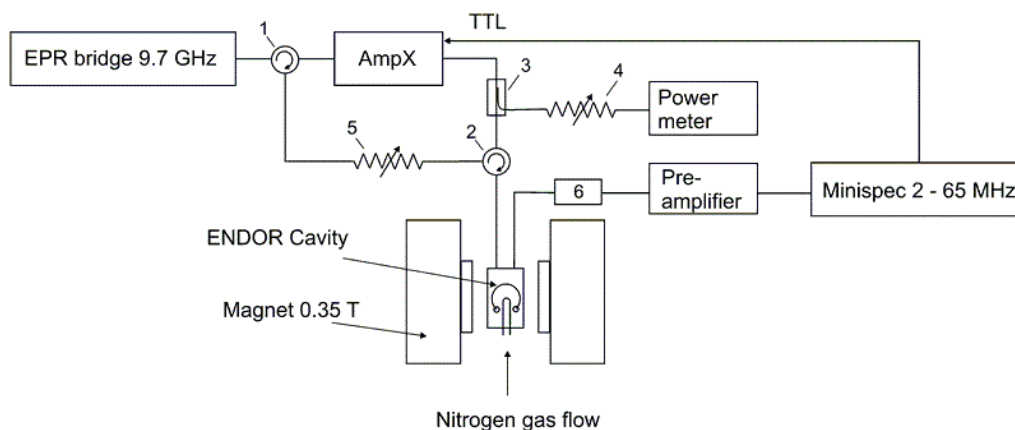
Figure 2.3. Simplified block diagram of an ESR spectrometer [31].

Magnetic coils are used to induce a large magnetic field of 0-6000 G in strength. In the Nuclear Magnetic Resonance (NMR) spectroscopy, the nuclear analog of ESR spectroscopy, signals are produced when frequency is varied across several megahertz

(MHz) while the magnetic field is kept constant on the sample to detect the chemical shifts associated with the signals. In the ESR spectroscopy, on the electron side, the resonant frequency is locked and the magnetic field is swept through the sample to record the signal to detect g factor associated with the signals. All ESR spectrometers are built on this method as it allows a better signal to noise ratio based on the microelectronics involved giving increased sensitivity. Such a configuration was possible with the surge in semiconductor based microelectronics research post World War II. The typical spectrum that is recorded is plotted as intensity versus field spectrum in the first derivative mode as shown in figure 2.1. The choice of using derivative mode in most commercial spectrometers is demanded by the microelectronics of system components, which gives a good signal to noise ratio for the recorded spectrum. The field axis of the spectrum reports the signal variations and resonance condition as the strength of the magnetic field increases, reported in Gauss (G) or milliTesla (mT). The intensity axis is related to the first derivative of magnetic susceptibility and many other spectrometer parameters, typically reported in arbitrary units due to several parameters involved in dependence. For the interested reader wishing to know more details about experimental techniques in ESR spectroscopy please refer to C P Poole, Electron Spin Resonance [28].

2.3 Typical lineshape of spectrum and its properties for Cu^{2+}

As mentioned in section 1.4, copper is ESR active in ground state and in +2 oxidation state, as both states have an unpaired spin associated with an electron. The normal non interacting isolated spin of copper would give a single resonance at ~3100 G (of the type shown in figure 2.1), corresponding to lone electron g factor of g_e=2.0023 (as per equation 3, [33, 34 and 35]) which would be a sharp derivative signal in ESR spectroscopy. However, copper also has a nuclear spin of I = $^3/_2$ which interacts with electron spin magnetic moment to give a hyperfine structure. Such hyperfine structure is theoretically expected to show **2I + 1** peaks, giving four peaks for copper center. The ESR spectrum of Cu^{2+} could be of three types such as normal spectrum, inverse spectrum or intermediate spectrum. We expect an ESR spectrum of normal type for these Cu^{2+} samples, also called the axial ESR spectrum, based on the g factor and associated parameters [32]. Hence, the Cu^{2+} center should show a typical spectrum as shown in figure 2.4. Based on the ligand field environment around the copper center, important information regarding the nature of copper center, its chemical environment, changes in species, etc effects can be either fully quantified or qualitatively interpreted from the ESR spectrum. Some of the important parameters that have been useful in this research exercise are described as follows.
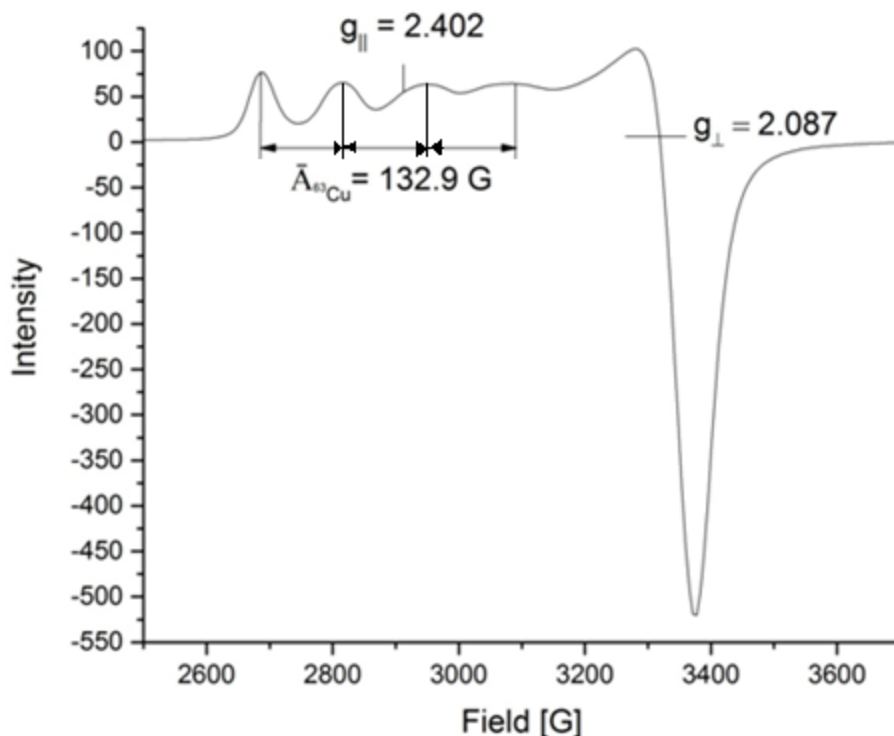
Figure 2.4. A representative ESR spectrum of one sample ("FAU IE 2.67 C" containing 2.67% Cu wt and calcined, recorded at ~4.2 K) studied for this research project. The various markings of g factor and average hyperfine splitting describe their calculation from the spectrum as detailed in section 2.3.3.

2.3.1 g factor

The g factor is a dimensionless number derived from the equation 1. The g factor, which is an empirical parameter [29], is a quantitative measurement of a molecule's magnetic moment formed by the spins on electrons. The g factor of a free electron is 2.0023 [33, 34 and 35] and the g factor of metal complexes is $\cong 2$ (as described by Wertz and Bolton [36]).

A simplified formula for g factor is given as [26],

$$g_i = 2.0023 \pm \frac{k\lambda}{E_0 - E_n} \qquad \text{equation 3}$$

here, k defines the degree of orbital mixing. For d^{1-4} λ is greater than 0 and for d^{6-9} λ is less than 0. Also, the result of $E_0 - E_n$ is negative. By convention therefore, the plus sign applies to more than half filled d orbitals and negative sign applies to less than half filled d orbitals. Hence, it is expected all the copper g factors reported here to be greater than 2.0023 [32].

IUPAC guidelines symmetrize the g factor across the three coordinate axes as g_x, g_y, g_z. Under formal IUPAC guidelines and in general scientific literature it is called as g matrix [37]. For a d^9 electronic system such as that of Cu^{2+} the g factor is split in two types - $g_x = g_y = g_\perp$ ie equivalent g tensor values along x and y axes and $g_z = g_\parallel$. Based on the geometry, spin system and specific ligand field environment there could be two possibilities at ground state when system is studied at low temperature - $g_\parallel > g_\perp$ or $g_\perp > g_\parallel$. An indicator of normal axial symmetric spectrum is $g_\parallel > g_\perp > g_e = 2.0023$ [32] wherein the unpaired spin points its resultant g factor in the z direction defined arbitrarily. The geometries that correspond to axial or normal spectra are elongated octahedral, square pyramidal or square planar which exhibit the ground state of $d_{x^2-y^2}$ orbital (D_{4h} local site symmetry) [32]. The g factor calculation method and assignments are explained in section 2.3.3.

2.3.2 Hyperfine coupling constant (A) and splitting (a)

The hyperfine coupling constant and splitting of the ESR spectrum when distinguished clearly allows the assignment of oxidation state of the paramagnetic metal center where

the unpaired electrons are delocalized with respect to the paramagnetic isotope source.

The hyperfine coupling constant and splitting can be directly interpreted from the ESR spectrum in field units or it can be converted to energy units to understand it from the molecular orbital energy level differences perspective. This hyperfine coupling constant for anisotropic systems is expressed mathematically as equation 4 based on the Zeeman energy terms and electron spin nucleus magnetic moment hyperfine coupling [38] as,

$$A = T + [Tr(A)/3] \, 1 \qquad\qquad \text{equation 4}$$

where A is a 3x3 hyperfine coupling matrix;

T is a traceless matrix (diagonal elements sum equals zero) and

1 is a 3x3 unit matrix.

The A cm^{-1} values are calculated by equating Electron Bohr Magneton (μ_e) with Bohr Magneton (μ_B) as per Dirac theory. Mathematically,

$$\mu_e = \frac{e\hbar}{2m_ec} = 9.274 \times 10^{-21} \text{ Erg/G} = 4.66864 \times 10^{-5} \text{ 1/cm G} \qquad \text{equation 5}$$

To convert hyperfine splitting in gauss to hyperfine coupling constant cm^{-1} we use [39],

$$A_{||_{63_{Cu}}} \text{ (cm}^{-1}\text{)} = a \text{ (G)}*g*\mu_e \qquad\qquad \text{equation 6}$$

The hyperfine coupling constant A is also a matrix like the g factor and is further diagonalized in x, y and z direction. For a d^9 electronic system, just like the g factor, the hyperfine coupling constant is split into $A_{||}$ & $A_{\perp}$. In many cases, the $A_{\perp}$ component of the hyperfine coupling constant may not be resolved clearly from the spectrum and it is calculated theoretically. For the experimental ESR spectroscopy, the hyperfine coupling constant $A_{||}$ and splitting parameter $a_{||}$ in relation with the g factor can help deduce significant information about a chemical system and its molecular picture. The hyperfine

splitting parameter (a) calculation method and assignments are explained as follows in section 2.3.3.

2.3.3 Calculation of g factors and hyperfine splitting

The g factor is split into two resultant factors – $g_{\parallel}$ and $g_{\perp}$. The $g_{\parallel}$ component is on the low field hyperfine for copper (II) system. It is calculated by taking the field value at the first hyperfine peak and last hyperfine peak and taking an average of it to get the value of B. Based on the correlation of g factor with magnetic field B and the frequency υ we can find $g_{\parallel}$ factor using a derived form of equation 1. The $g_{\perp}$ factor is calculated at node field value. The hyperfine splitting a is calculated in field units by taking an average of the hyperfine peak field values. For spectrum shown in figure 2.4, at field value of 2885 G $g_{\parallel}$ = 2.402 (±0.001), at field value of 3319 G $g_{\perp}$ = 2.087 (±0.001) and hyperfine splitting $a_{\parallel_{63_{Cu}}}$ = [3084.1 - 2685.3) / 3] = 132.9 G (±3 G).

2.4 Application of ESR in copper doped zeolites

As mentioned previously, ESR is the most powerful analytical tool in characterizing the local environment of systems containing unpaired electrons. The advantage of studying copper doped zeolites by this method is that the copper reaction center for catalytic activity in NH_3 SCR catalysis gives a distinct ESR signal in +2 oxidation state [17]. Currently, the local environment of this metal center (eg coordination geometry,

average oxidation state and ligand field identity) is not very well understood and significant research efforts have been dedicated to understand this catalytic species [21-24, 41 and 43]. Hence, for the current research exercise, we extensively utilize ESR spectroscopy to understand the nature of copper in faujasites and chabazites by subjecting it to several treatment conditions and interpret the results based on existing literature [26, 30 and 42-46] for copper exchanged zeolites and inorganic chemical knowledge for copper in different systems of similar interest. We can interpret ESR results for copper in faujasites & chabazites with less ambiguity since the only ESR detectable site is the copper centers. The local ligand field environment around copper center influences the ESR signal [46]. Other components of the zeolitic framework are ESR silent and this helps eliminate spurious signals or a relatively complex spectrum that would otherwise require computational simulations for the assignment of signals based on established spin Hamiltonian models [36]. Hence, ESR spectroscopy can shed significant light on the relatively perceived simple system of copper exchanged zeolites with many important industrial applications, most important being NH_3 SCR catalysis.

3. Experimental

3.1 Synthesis procedures for copper doped zeolites

3.1.1 Ion exchange process (IE)

The zeolite precursors were procured from Zeolyst International for faujasite (Si/Al = 2.6 of Y type) and chabazite (Si/Al = 15 of SSZ-13 type) by BASF. Copper doping may be achieved through three established methods viz ion exchange, wet mixing and impregnation [40]. Many literature reports (representative eg [40-43 and references therein]) have indicated superiority of ion exchange method in achieving high conversion of NO_x gases to N_2. Hence, we used ion exchange method [40] for introducing copper in zeolites for most samples. Copper nitrate or acetate salts (Alfa Aesar) were used as copper source by BASF. The ion exchange process was carried out at 60 ℃ by stirring the zeolite powder and predetermined amount of the salt in deionized water for varying durations by BASF. The slurry was filtered and washed in aliquots of deionized water and then dried overnight in an oven at 85 ℃ by BASF.

The samples obtained after this treatment were designated "as dried" samples with varying copper loading viz 2.6, 3.6 and 5.3 % Cu wt determined by ICP-AES analysis by BASF. The sample labels are described in table 2.

3.1.2 Precipitation method (P)

An alternate precipitation method, which is a modification of the impregnation method, was utilized to study the nature of copper (II) centers in them. One alternate sample, of the Y type zeolite from faujasite family, same as zeolites used for the ion exchange method, was prepared via precipitation method by BASF. This sample had ~2.4% elemental copper weight as determined by ICP AES analysis by BASF. Additionally, a sample from the chabazite family of zeolites with SSZ 13 framework type was also prepared by precipitation method [40] giving 2.2% Cu wt (Si/Al = 15) as determined by ICP AES analysis by BASF. The sample labels are described in table 2.

3.2 Treatment procedures for copper doped zeolites

3.2.1 Calcination (C)

Three samples were subjected to calcination treatment. First, one representative "FAU IE 2.67 C" from the "as dried" type after ion exchange method was subjected to calcination treatment at 450℃ for 2 hours in a tube type of furnace. Second, the precipitated sample "FAU P ~2.4 C" was further subjected to calcination treatment at 450℃ for 2 hours. Third, a chabazite type sample "CHA P 2.2 C" was calcined at 450℃ for 2 hours. The sample labels are described in table 2.

3.2.2 Hydrothermal aging

The chabazite type of calcined sample was subjected to hydrothermal treatment by steam aging the samples at 750℃ with steam at ambient pressure and 10% percent water. This hydrothermally aged sample was labeled as "CHA P 2.2 S" with 2.2% copper weight as determined by ICP AES analysis by BASF. The sample labels are described in table 2.

Table 2. Sample details summary.

Sample Cu wt %	Sample ID (Zeolite, synthesis method, % Cu wt & treatment)	State	Si/Al
2.6	FAU IE 2.6	as dried	2.6
3.6	FAU IE 3.6	as dried	2.6
5.3	FAU IE 5.3	as dried	2.6
~2.4	FAU P ~2.4 C	calcined	2.6
2.67	FAU IE 2.67 C	calcined	2.6
2.2	CHA P 2.2 C	calcined	15
2.2	CHA P 2.2 S	hydrothermally aged	15

3.3 Sample preparations for ESR based measurements

All samples were measured as powder samples. The powder samples were taken as it is without any pretreatment. A suprasil quartz grade ESR tube of 3 mm inner diameter/ 4mm outer diameter of 707 SQ type from Wilmad Labglass were used for all ESR measurements. All samples were measured as 'line samples' for ESR. A 'line sample' is one that covers the active region of ESR resonator cavity fully to avoid sample position specific measurements. The microporous zeolite samples were densely packed in ESR tube by tapping the tube end a few times on lab bench top. The samples were fixed in position by using a small cotton plug. Such prepared tubes were then capped with a plastic cap to avoid introduction of moisture and foreign particles, they can also be sealed permanently. At high or low temperature measurement, the samples were uncapped briefly during the measurement. This uncapping was necessary to allow the escape of trapped air and adsorbed moisture at high temperature, accommodate instrument restrictions and to allow escape for trapped air when contraction occurs due to low temperature.

3.4 Measurement conditions and set up for ESR spectroscopy

All ESR measurements were performed in continuous wave X band frequency (~9.5 GHz frequency) operation. All experiment specific instrument parameters are given in

appendix B. Four temperature conditions used for ESR measurements to probe copper microenvironment are detailed below.

3.4.1 Room temperature ESR measurement

All room temperature measurements were done using either Elexsys E580 spectrometer with ER 4102 ST resonator (of rectangular construction) or EMX+ spectrometer in X band configuration with EMX+ Microwave Bridge and an ER 4119 HS cavity (of cylindrical construction) from Bruker corporation. The sample was positioned centrally using best physical estimate of active microwave region in the cavity in an ESR quartz tube manufactured by Wilmad. The signal processing and data processing software used for recording data and spectral calculations is either XEPR or Xenon provided by Bruker corporation.

3.4.2 High temperature ESR measurement

For high temperature measurement, in addition to room temperature setup described in 3.4.1, a transfer line embedded with heating coils was used. Nitrogen gas was passed through this transfer line connected to ER 4102 ST through a dewar to heat up the sample. Temperature was controlled through ER 4111 VT variable temperature controller.

3.4.3 Low temperature ESR measurement at ~100 K

A low temperature of ~100 K was achieved through use of liquid nitrogen in a storage dewar containing a heating element (from Bruker) and connected to a silvered transfer line. This transfer line was connected to ER 4102 ST resonator through a dewar. Cold gaseous nitrogen was passed through sample to achieve a stable temperature of ~100 K. Temperature was controlled through ER 4111 VT (from Bruker) variable temperature controller. A Thermocouple (Cu Co, T type) was calibrated using room temperature reference.

3.4.4 Low temperature ESR measurement at ~4.2 K

A low temperature of ~4.2 K was achieved through use of liquid helium from Airgas. An ESR 900 cryostat for Oxford instruments was used with ER 4102 ST resonator connected to helium source through a GFS 300 transfer line from Oxford instruments. Alternatively, an ER 4118 CF resonator from Bruker Corporation with CF 935 O cryostat from Oxford instruments were used for measurement of some samples. A rotary pump and flow controller were used to control the flow of super cooled helium gas through vacuum pressure. All measurements were under continuous flow conditions. Temperature control was achieved through ITC 502 variable temperature controller from Oxford instruments. The temperature controller thermocouple for helium based measurements was calibrated using liquid nitrogen reference.

4. Results and Discussions

The results and discussions are organized based on sample condition with respect to treatment viz as dried samples, calcined samples, precipitated samples and higher Si/Al ratio samples described below. All spectra reported here are without baseline on either side. All ESR measurement specific parameters are listed in detail in appendix B.

4.1 Ion Exchanged samples

Three samples – FAU IE 2.6, FAU IE 3.6 and FAU IE 5.3 were measured in "as dried" condition without any further treatments. Multiple measurement conditions and ESR spectrum based analysis techniques were employed to understand the nature of copper in these samples described as follows.

4.1.1 Room temperature ESR measurement on ion exchanged samples
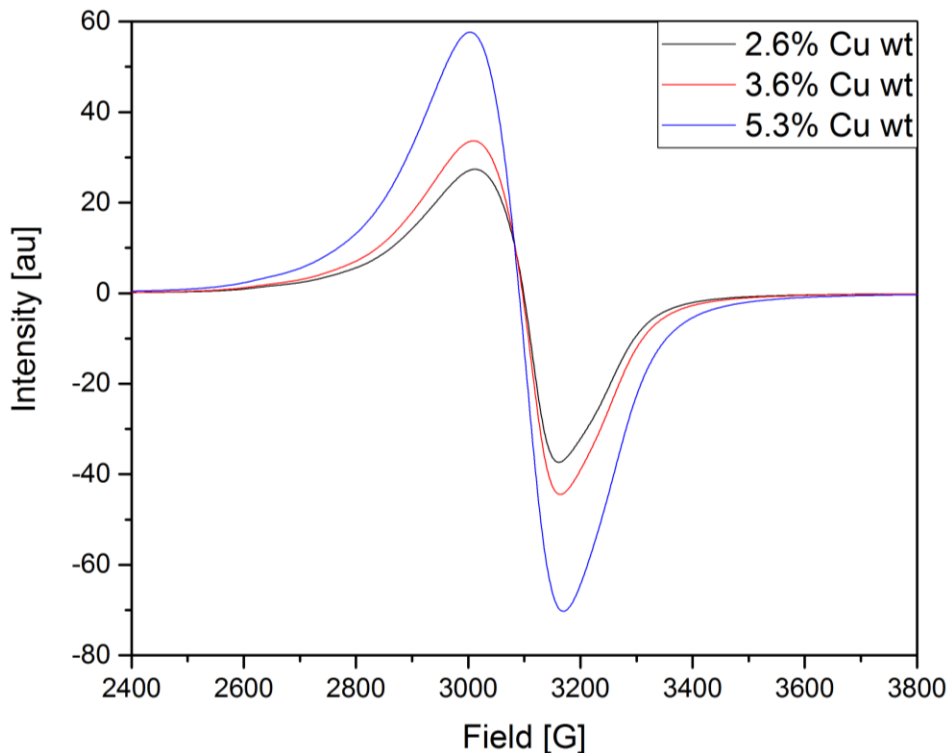
Figure 4.1. 1D field sweep across the field strength varying from 100 – 6100 G (1 T = 10-4 G) is shown here only for the active region in which signal was observed at room temperature (~298 K) for FAU IE 2.6, FAU IE 3.6 and FAU IE 5.3.

The "as dried" samples measured at room temperature (~298 K) gave an almost isotropic symmetrical spectrum with indistinguishable hyperfine as expected at room temperature due to thermal spin dependent behavior at high temperatures as per the Boltzmann distribution given in equation 2. In figure 4.1 above, we note that increasing copper weight percent in synthesized samples contributes to increase in intensity.

4.1.2 Low temperature ESR measurement at ~100 K on ion exchanged samples
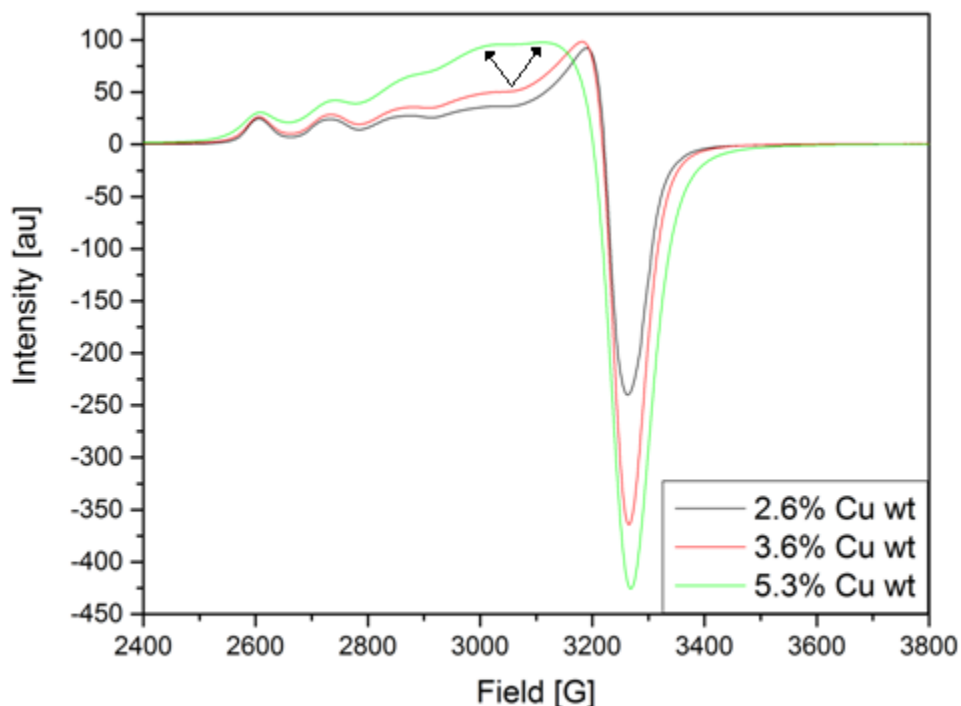
Figure 4.2. 1D field sweep spectrum performed on ion exchanged samples – FAU IE 2.6, FAU IE 3.6 and FAU IE 5.3 cooled to ~100 K.

The "as dried" samples (FAU IE 2.6, FAU IE 3.6 and FAU IE 5.3) measured at ~100 K shown in figure 4.2 clearly shows the typical hyperfine spectrum for [63]Cu. The hyperfine is resolved only on the low field side with two well resolved peaks and the third and fourth peaks are successively more broadened. Special features for 5.3 % copper weight are pointed out with arrows. To resolve this hyperfine further and understand its temperature dependence we go to a lower temperature of ~4.2 K.

4.1.3 Low temperature ESR measurement at ∼4.2 K on ion exchanged samples
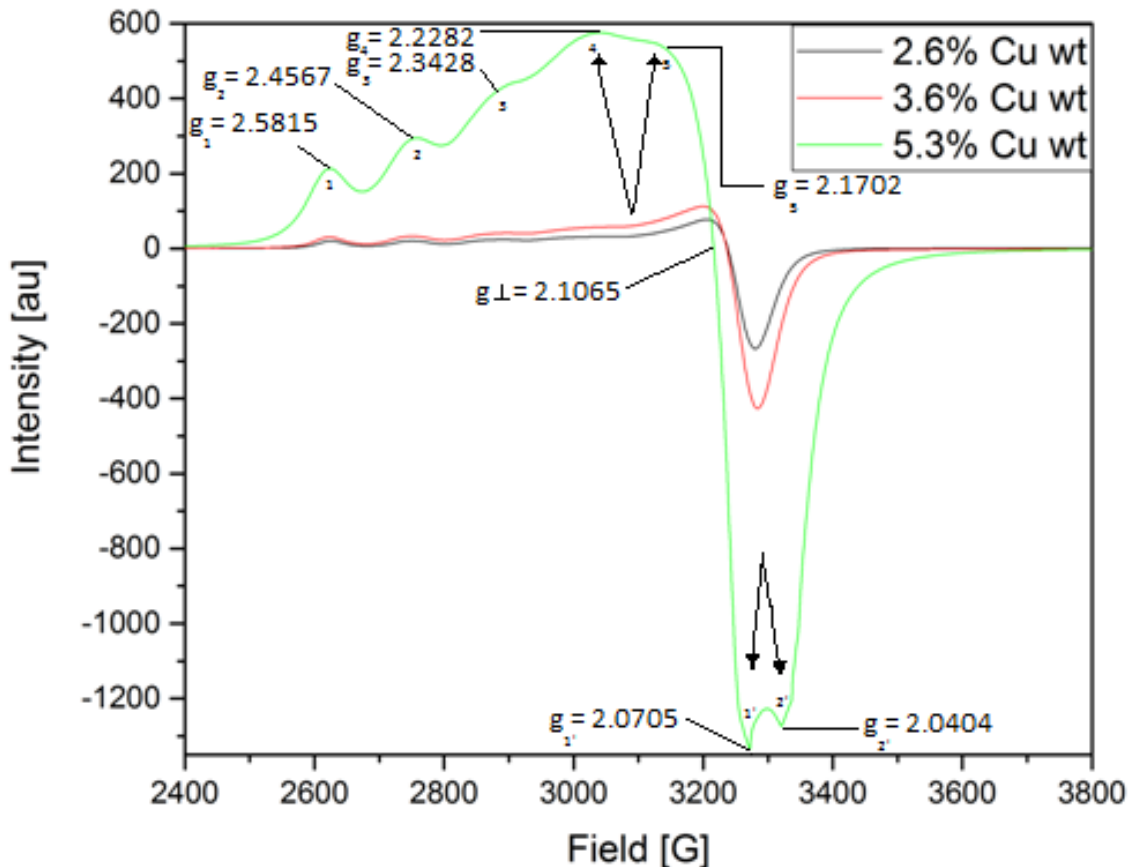
Figure 4.3. 1D field sweep spectrum performed on ion exchanged samples – FAU IE 2.6, FAU IE 3.6 and FAU IE 5.3 cooled to ∼4.2 K.

As described above in equation 2, based on Boltzmann temperature distribution constant, lower temperature allows better resolution (∼1000 times) of energy states of a system. The spectrum recorded at ∼4.2 K is reported in figure 4.3 for three samples with 2.6, 3.6 and 5.3 % copper weight. The spectra show the same g factors and hyperfine peak locations up to 3.6 % Cu wt with an increase in intensity that is based on detected copper (II) loading. At 5.3 % Cu wt, the spectrum changes sharply with several

additional features (figure 4.3 and relevant g factors noted therein). These features are not seen at higher temperatures or lower copper loadings. Such features are indicative of a change in symmetry of copper center from axial to non axial symmetry [32]. This non axial symmetry feature is also known as rhombicity and the spectrum is called as rhombic spectrum. In addition, the major peak at which the signal changes to trough is merging with the fourth hyperfine peak to give a sharp peak. On the high field side, we see an added hyperfine splitting allowing resolution of the hyperfine splitting.

These spectral features were also observed at $\sim$100 K on the low field side; however, the sharp increase in intensity at $\sim$4.2 K for 5.3 % Cu wt indicates non Curie temperature dependent spin behavior deviating from linear behavior of spin based on varying temperature. This suggests two different ESR active copper centers are located in the zeolites. The regular signal is contributed by copper located in zeolite cage at its preferred site that allows the rapid reversible exchange of ligands to reduce NO_x gases based on low electrostatic redox potentials. We propose the second, g < 2.07 feature implying copper in rhombic symmetry, may be contributed by copper located in zeolite defects made pronounced by change in geometry due to constriction at the binding site and broadening of peak to trough transition. Since any spectrum is averaged over multiple active centers, the resulting spectrum represents the features of all such centers.

The low field region does not show any signal in the field region of $\sim$1500 G (not reported here). This indicates absence of any weakly coupled binuclear clusters that may have been formed in these samples. Given the consistency of the spectral features

at all other temperatures for lower copper loading it appears that speciation is the case here. Such speciation is temperature dependent indicating thermal mobility of copper centers. Further elaboration is as follows discussing the effects of calcination on similar samples and hydrothermal aging performed only on the 2.2S sample with chabazite framework.

4.2 Calcination treatment

A sample from the faujasite Y type of zeolite labeled as "FAU IE 2.67 C" was studied for the effect of calcination. It is a representative of the "as dried" sample family and comparisons are established vide infra. It was measured at multiple temperature levels as discussed below.

4.2.1 Room temperature (∼298 K) ESR measurement of "FAU IE 2.67 C" sample
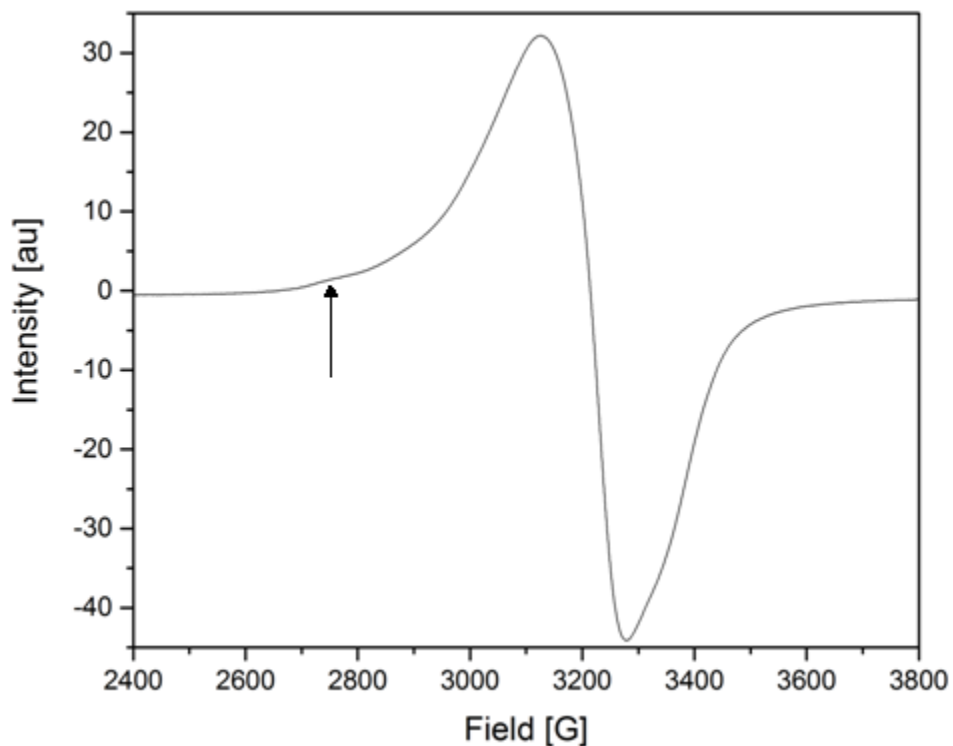
Figure 4.4. A room temperature 1 D field sweep spectrum for the "FAU IE 2.67 C" sample.

At room temperature, the "FAU IE 2.67 C" calcined sample gave symmetric signal in the field region of 2400-3800 G. There is no distinguishable hyperfine structure visible except a slightly appearing first peak at ~2800 G shown in figure 4.4. There is no rhombicity seen on the high field side though broadening on the high field side is observed.

4.2.2 Low temperature ESR measurement at ~100 K on "FAU IE 2.67 C" sample
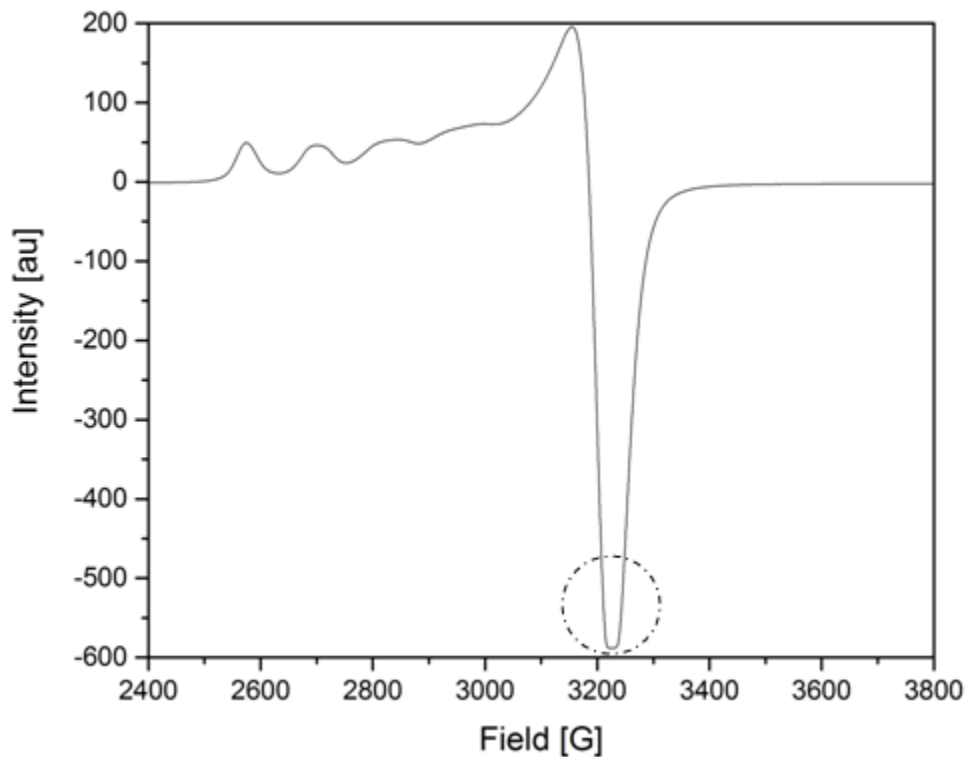
Figure 4.5. A 1D field sweep spectrum of "FAU IE 2.67 C" sample cooled to ~100 K.

At low temperature of ~100 K using liquid nitrogen, we were able to resolve the hyperfine structure of copper as shown in figure 4.5. A clearly visible four peak hyperfine associated with ^{63}Cu is observed with well resolved first and second peaks and broadened third and fourth peaks. A broadened $g_\perp$ feature is noted however (encircled in figure 4.5), it was not resolved further here. The spectrum indicates symmetric axial geometry.

4.2.3 Low temperature ESR measurement at ~4.2 K on "FAU IE 2.67 C" sample
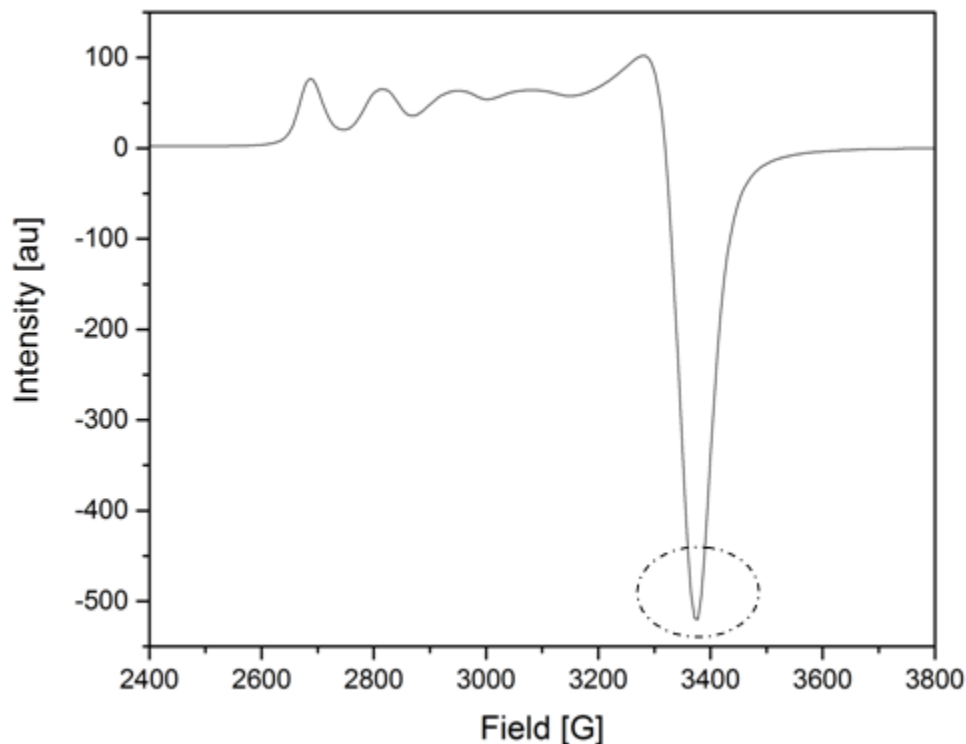
Figure 4.6. A 1D field sweep spectrum for "FAU IE 2.67 C" sample cooled to ~4.2 K.

At low temperature (~4.2 K) using liquid helium, a well resolved spectrum is obtained as shown in figure 4.6. At this low temperature, the spectral features are distinct and ESR parameters can be ascertained such as $g_\parallel$, $g_\perp$ and $a_\parallel$ as reported in appendix table B. A slight change in resolution of hyperfine structure is observed where the four peaks are well resolved albeit with increasing broadening but comparatively better than that observed at liquid nitrogen analysis at ~100 K. On the high field side, the trough is sharp (encircled in figure 4.6) compared to a broadened feature seen in figure 4.5 (encircled) for ~100 K spectrum. Such features are consistent for a ^{63}Cu center in approximate D_{4h} axial symmetry and with minimal thermal influenced change of geometry [30, 32, and

47]. On comparing this spectrum with the spectrum for "as dried" samples, we see consistency in spectral features and the identity of ESR active species to be ^{63}Cu with a four coordinate geometry. Hence, we can say that calcination effect has not changed the physical nature of copper in these zeolites in significantly measureable proportions.

4.3 Effect of precipitation method for synthesis

An alternative synthesis technique of precipitation was used for synthesis as described in section 3.1.2 for the Y type of zeolite with Si/Al = 2.6 copper doping. This sample labeled "FAU P ~2.4 C" was analyzed to study the change of synthesis method effect on nature of copper. This sample showed major changes from the spectrum for calcined sample discussed in section 4.2.1 and figures 4.4, 4.5 and 4.6. The details of the spectrum at different temperature levels are described vide infra.

4.3.1 Room temperature ESR measurement on "FAU P ~2.4 C" sample
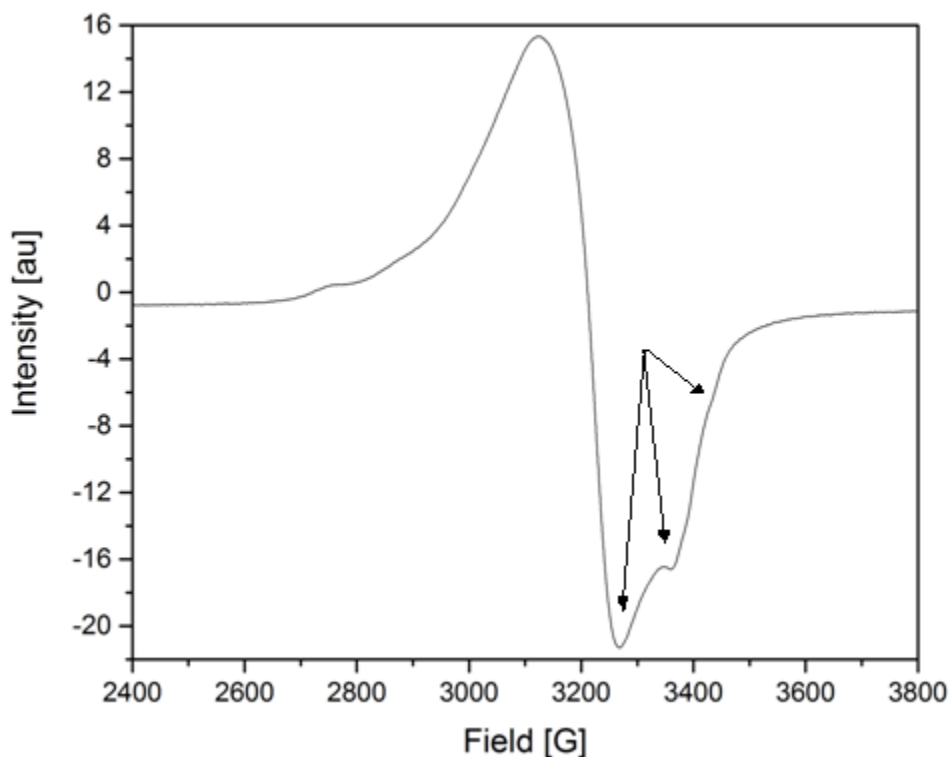
Figure 4.7. 1D field sweep spectrum of "FAU P ~2.4 C" measured at room temperature.

Rhombicity is prominent even at room temperature for the copper precipitated in zeolite for this sample. As seen from figure 4.7 the prominent rhombic feature appears at ~3350 G and a broadened feature at ~3475 G. We also see two slight bumps on the low field side, at ~2750 & ~2900 G indicating partial resolution of [63]Cu hyperfine. The odd trough at the right can be described by classifying the spectrum as intermediate type [32]. This kind of spectrum suggests penta coordinated Cu2+ ion with square pyramidal or trigonal bipyramidal geometry [32]. We investigate the effect of precipitation in this sample further, by probing it at lower temperature levels.

4.3.2 ESR measurement of "FAU P ~2.4 C" sample at ~100 K
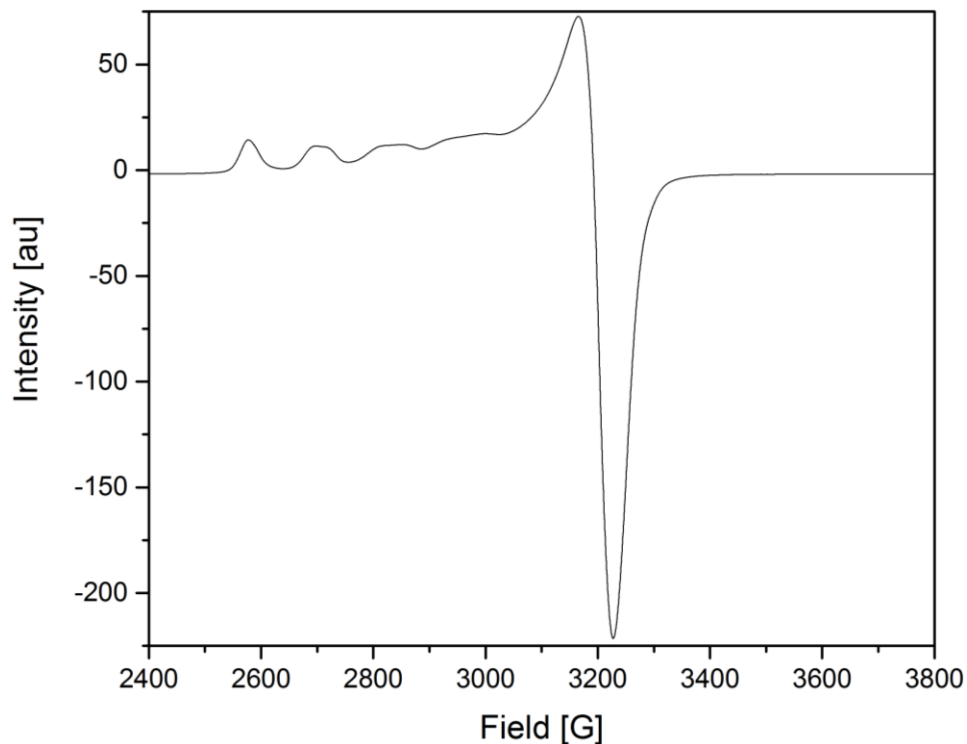
Figure 4.8. 1D field sweep spectrum of "FAU P ~2.4 C" in calcined state at ~100 K.

At ~100 K using liquid nitrogen, we see the common spectrum with four peaks hyperfine for [63]Cu state reappearing. This indicates that the copper is mobile rather than fixed in the zeolite framework for the precipitated sample showing change in spatial distribution. The reorganization of copper center has occurred through a change from asymmetric (rhombic) to symmetric axial geometry. It is difficult to comment on specific chemical changes such as full identity of changing coordinating ligands solely based on the CW ESR spectrum, however, such changes cannot be ruled out in this case.

4.3.3 ESR measurement of "FAU P ~2.4 C" sample at ~4.2 K
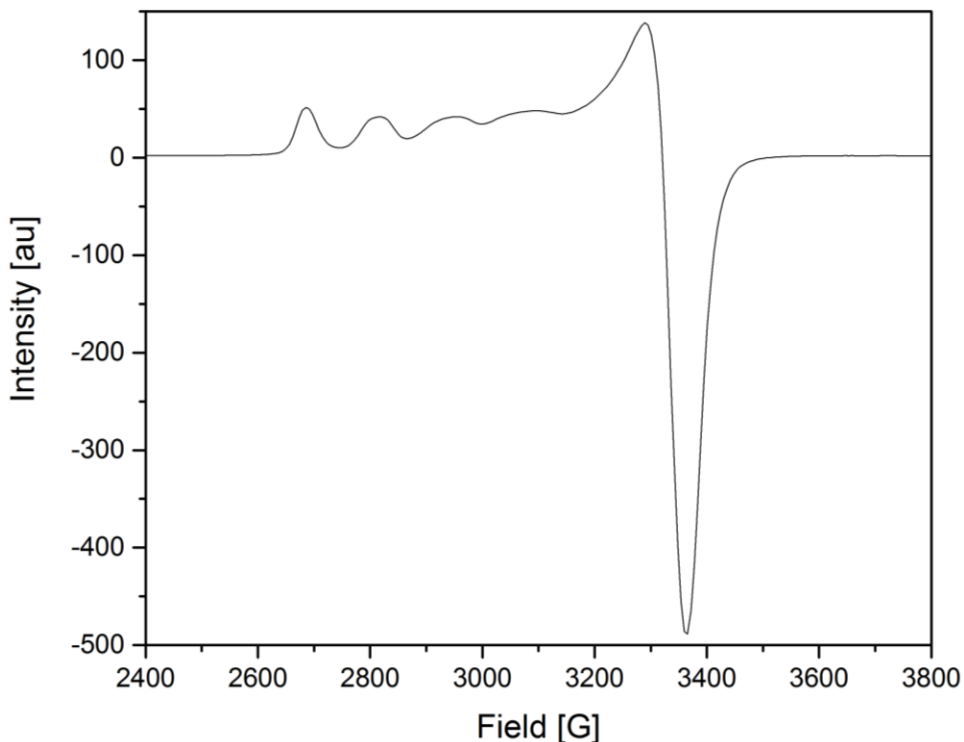
Figure 4.9. 1D field sweep spectrum of "FAU P ~2.4 C" sample recorded at ~4.2 K.

We probed the copper center in precipitated sample "FAU P ~2.4 C", at a further lower temperature of ~4.2 K. At this low temperature, we expect the relaxation time of the spin to be increased significantly to allow detection of ground state of spin and its neighboring environment. The spectrum, as reported in figure 4.9, is consistent in hyperfine on the low field side and the high field side with the low temperature spectrum reported in figure 4.8. Ignoring the temperature dependent increase in intensity by going for a low measurement temperature, the spectrum does not indicate any detectable speciation for copper center that is consistent with uncalcined ion exchanged samples at low temperature. The hyperfine structure here is further resolved

with clear peaks though broadened indicating effect of ligand field on the Cu^{2+} center. This spectrum is indicative of a typical four coordinate geometry for copper center indicative of its mobility when compared with room temperature spectrum.

Hence, the copper precipitated in zeolites is thermally mobile and initially deposited at non-regular site that imposes stereo specific hindrances on it, which are minimized at lower temperatures by change in site.

4.4 Altered zeolite framework and Si/Al ratio

Two samples – "CHA P 2.2 C" and "CHA P 2.2 S" were prepared from chabazite type of zeolite to study the nature of copper in a different zeolitic framework with significant change in Si/Al ratio, from Si/Al = 2.6 for samples studied earlier to Si/Al = 15. These two samples were prepared by precipitation method as described in section 3.1.2 to probe further the thermal mobility of copper centers in zeolite structure. Further, these samples were subjected to calcination and hydrothermal aging treatments to study the degrading effects on copper center when exposed to severe conditions typically subjected to NH_3 SCR catalysts in mobile applications. Hydrothermal aging via exposure to steam at high temperature simulates the environment of diesel engines under which these catalysts should retain high NO_x gas conversion functionality. Two samples, both containing 2.2 % elemental copper weight, were probed to understand the dependence of temperature and treatment conditions. Their analysis is summarized vide infra.

4.4.1 Effect of calcination on sample with higher Si/Al zeolite ("CHA P 2.2 C")
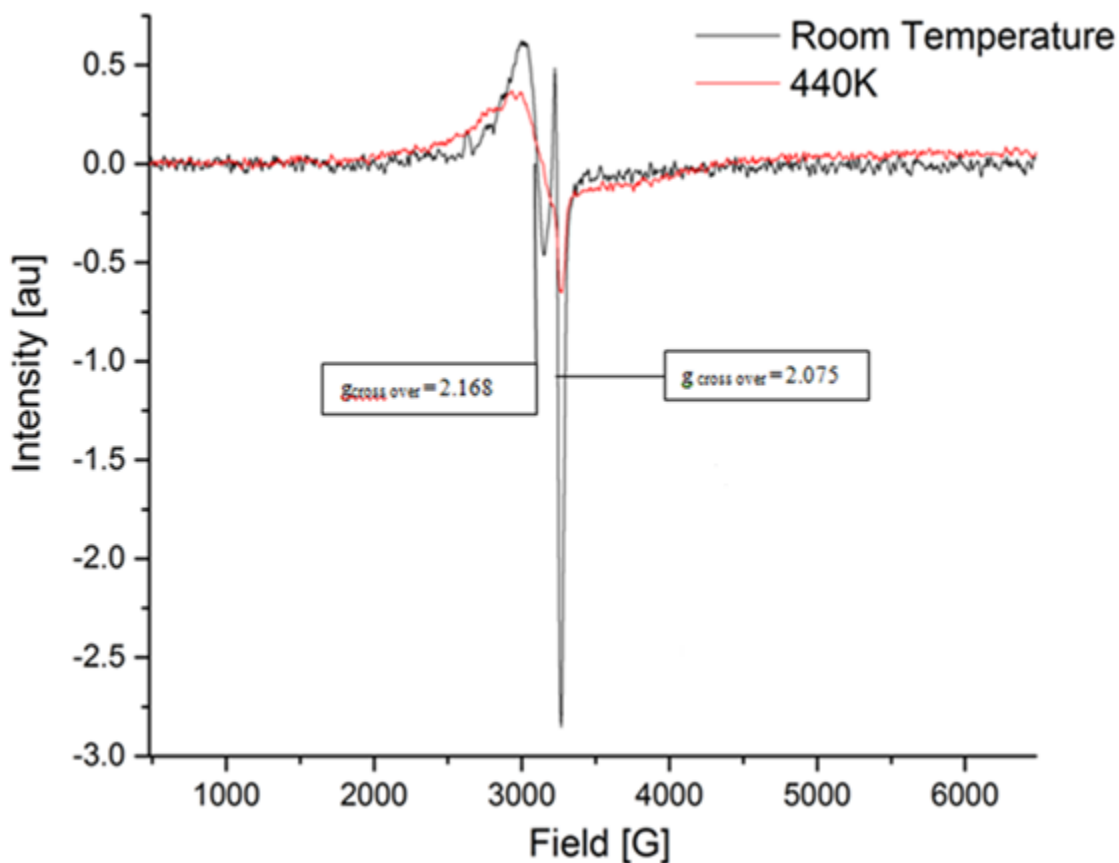
Figure 4.10. Effect of calcination on "CHA P 2.2 C" sample with higher Si/Al zeolite measured at room temperature (black) and at ~440 K (red) reported as a 1D field sweep spectrum.

The calcined sample with higher Si/Al gave an ESR spectrum shown in figure 4.10 of very low signal to noise ratio (S/N ~15 at 298 K or room temperature and S/N ~123 at ~440 K) compared to other spectra reported here so far for copper in zeolite system. The spectrum at room temperature, figure 4.10 black spectrum, shows a sharp signal at ~3250 G with small peak to peak width of 41 G ($\pm$3 G) in comparison to broad peak spanning ~2750-3200 G, with a peak to peak width of 153 G ($\pm$3 G). On the low field

side, for the broad peak, a slightly distinguishable hyperfine structure is observed. Hence, it appears a case of speciation of copper center.

To understand these changes in copper center we employed a high temperature experiment and detected significant changes from room temperature spectrum. At a high temperature measurement of ~440 K (167℃) we observe that the copper center has degraded significantly indicated by apparent decrease in intensity, as shown in the red spectrum in figure 4.10. Such degradation can theoretically be correlated with Boltzmann distribution given in equation 2. Moreover, the spectrum has broadened significantly to merge the two distinguishable peaks into one broad peak with hardly distinguishable features. We note the appearance of hyperfine observed at room temperature on the broad peak is no longer visible. The identity of the second species is retained to some degree as observed on the trough side at ~3200-3400 G. This part of the spectrum overlaps well with the same part of the room temperature spectrum, which indicates change in speciation is temperature dependent for copper center in these samples. Hence, for the copper precipitated sample "CHA P 2.2 C", two types of copper centers are observed with ESR in a highly temperature dependent state.

4.4.2 Effect of hydrothermal aging on sample with higher Si/Al zeolite ("CHA P 2.2 S")
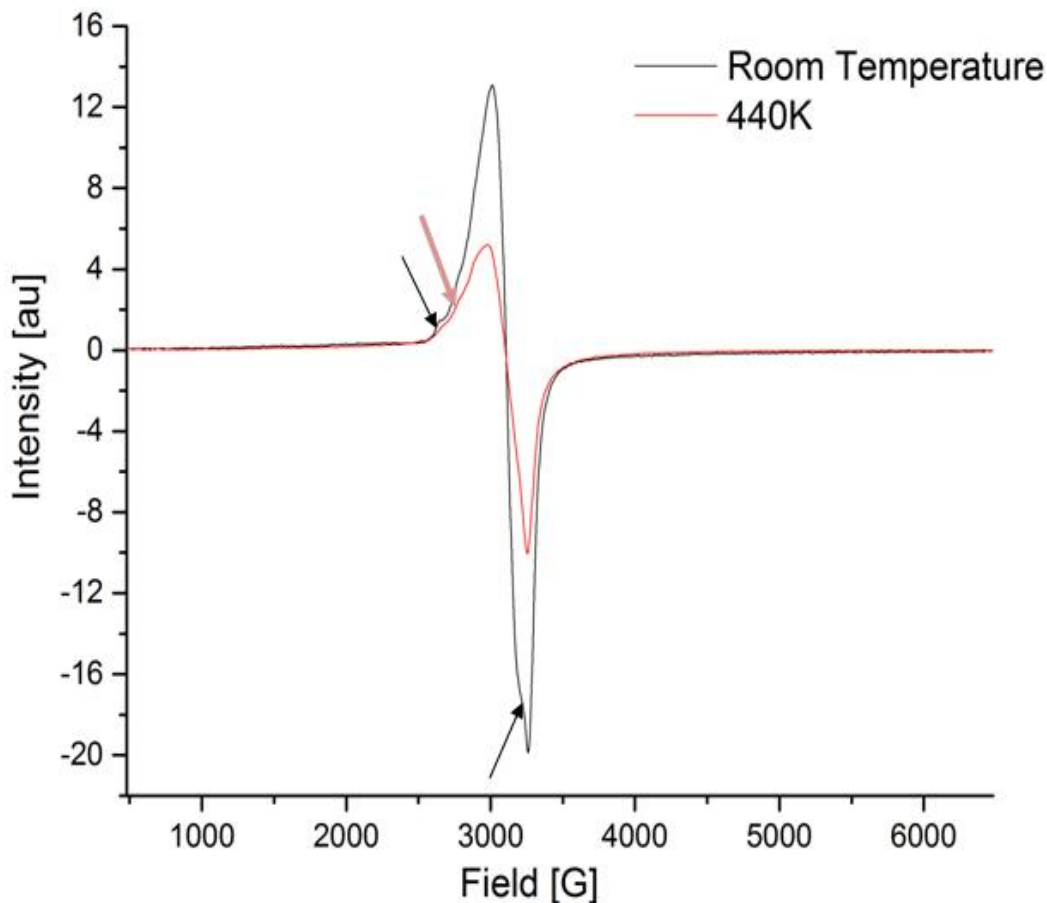
Figure 4.11. Effect of hydrothermal aging on "CHA P 2.2 S" sample with higher Si/Al zeolite measured at room temperature (in black) and at ~440 K (in red) reported as 1D field sweep spectrum.

The copper precipitated chabazite sample was subjected to a hydrothermal aging treatment as described in section 3.2.2. In figure 4.11, at room temperature (in black), the spectrum hardly indicates any g anisotropy with faintly recognizable hyperfine peaks appearing on the low field side. On the high field side, at ~3200 G, we see sharpening of the signal towards approaching trough transition on the lower intensity side. This may

be indicative of emergence of rhombicity. At ~440 K, the spectrum retains features of room temperature spectrum with decrease in intensity. On the low field side for spectrum at ~440 K, the hyperfine peaks are slightly visible but broadened significantly. On the high field side for spectrum at ~440 K, the sharpening of trough is consistent, indicating the merging of two formed species, if any. On comparing the spectrum for steam aged sample with calcined sample for Si/Al = 15 chabazite in figure 4.10, the speciation of copper has reduced in steam aged sample to almost negligible content since it does not show a distinct signal for second species, rather the signal in this case in merged into one consistent signal. A broader comparison with signals recorded for "as dried" & "calcined" samples of faujasite family in sections 4.1 and 4.2 respectively indicate consistency in the identity of the active center being ^{63}Cu based on the region of the peak to trough transition in field. This indicates that significant changes in spectral features are a contribution of specific ligand field to which the copper center is exposed. Hence, we rule out the possibility of a heterogeneous species contributing to signal such as O_2. The spectrum is an intrinsic copper spectrum with changes in intensity and lineshape attributed to loss or rapid exchange of ligands such as H_2O (aqua), OH^- or O^- with zeolite framework oxygen [41].

4.4.3 Simultaneous comparison for calcination ("CHA P 2.2 C") and steam aging ("CHA P 2.2 S") effects
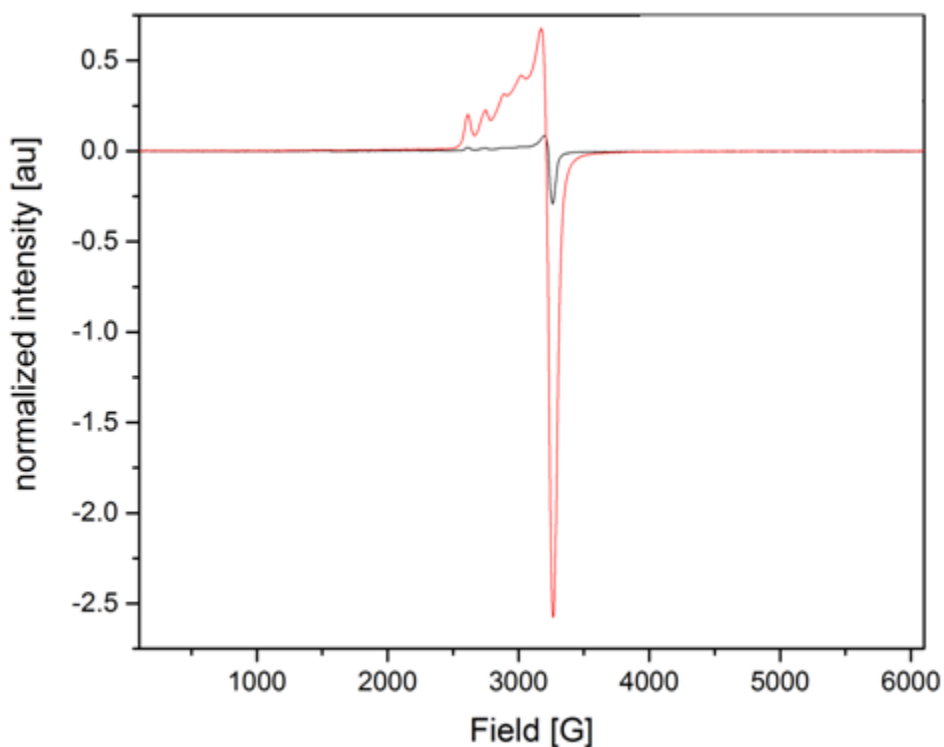
Figure 4.12. A comparative analysis of hyperfine structure for samples, of 2.2% elemental copper weight, with calined (black) and hydrothermally aged (red) treatments measured at ~95 K. The intensity scale is normalized for the ESR parameters that were used for measurements at room temperature and ~440 K for a comparative analysis. Refer appendix table B for ESR parameters.

A good simultaneous comparison for calcination and aging treatments can be done at a low temperature of ~100 K using liquid nitrogen to increase the relaxation time of spins as discussed previously (refer equation 2 and its discussion). The calcined and steam aged samples with higher Si/Al were measured at ~95 K and plotted in figure 4.12. Both

spectra show typical [63]Cu four peak hyperfine on the low field side with no special features on the high field side. The spectrum for calcined sample is diminished significantly in intensity in comparison to steam aged sample. Due to isolation of copper in ground state at this low temperature, a direct temperature based comparison is more suitable here for these samples. Stronger evidence for thermal mobility of copper centers is ascertained by these test results. The change of copper center from asymmetric to symmetric spectra with well resolved hyperfine peaks indicates mobility of copper center occurring due to temperature and to overcome stereo specific hindrance offered to it, when compared to unhindered ion exchanged samples.

4.4.4 Spin behavior analysis for alternate Si/Al ratio samples

The number of spins for a paramagnetic sample is calculated from the spectrum by taking double integration of the actual signal eliminated from baseline. Such double integration gives the amplitude of the signal. Some normalization for reported amplitude may be inevitable based on the quality factor of resonator tuning (Q factor) and the temperature of measurement. On comparing such normalized spins versus the temperature of measurement, we can understand the spin behavior of copper centers in these samples as Curie paramagnets. The spin behavior analysis for calcined and steam aged is discussed as follows.

4.4.4.1 Spin behavior of calcined sample "CHA P 2.2 C"

Figure 4.13. Spin dependence on temperature for 2.2 % elemental copper weight sample "CHA P 2.2 C". Y axis is the double integration area of derivative ESR spectrum divided by resonator Q factor for normalization. Refer table B in appendix for details.

The total spins obtained after double integration of spectrum at ~95 K, room temperature (~298 K) and ~440 K when normalized for Q value and plotted against temperature of measurement showed an almost linear behavior as reported in figure 4.13. The ratio of intensity of calcined sample measured at ~95 K to room temperature is 0.076. Spectral parameters have influenced this loss in intensity; however, the features of hyperfine are consistent with regular Cu^{2+} state. Typically, we expect the spins to decrease at elevated temperatures for Curie paramagnets. The abnormal

increase in spins from room temperature to ~440 K may be due to signal broadening arising out of rapid spin transitions with change in geometry of the copper centers. The spins in the excited state at higher temperature are aligned in the unpaired state leading to increased number of spins with independent g factors (x, y and z) being additive. Possibility of phase change associated with spin cannot be ruled out, such as change from +2 to +1 oxidation state for copper center.

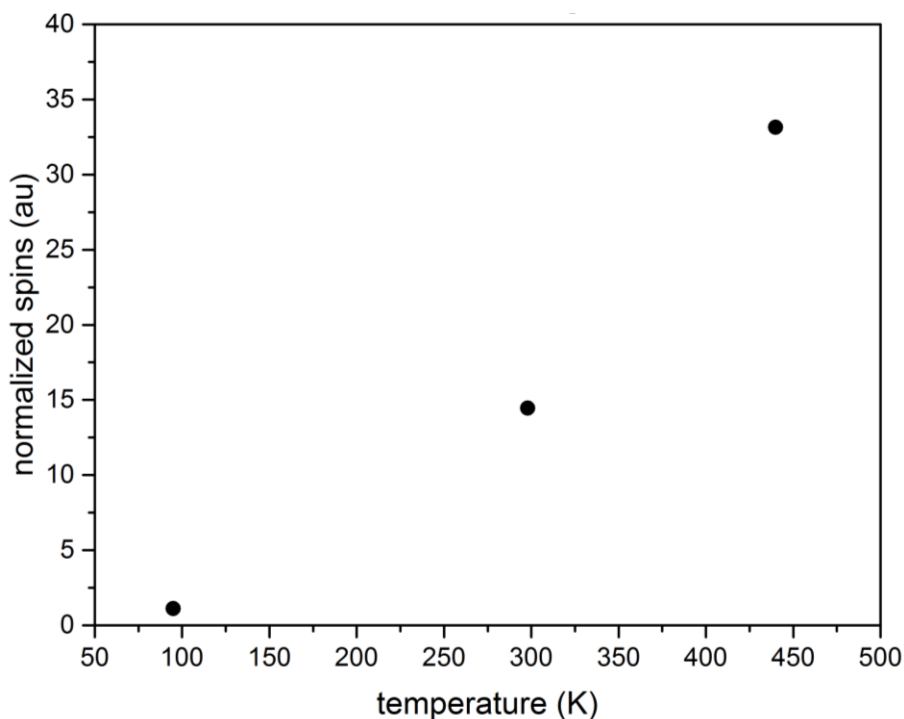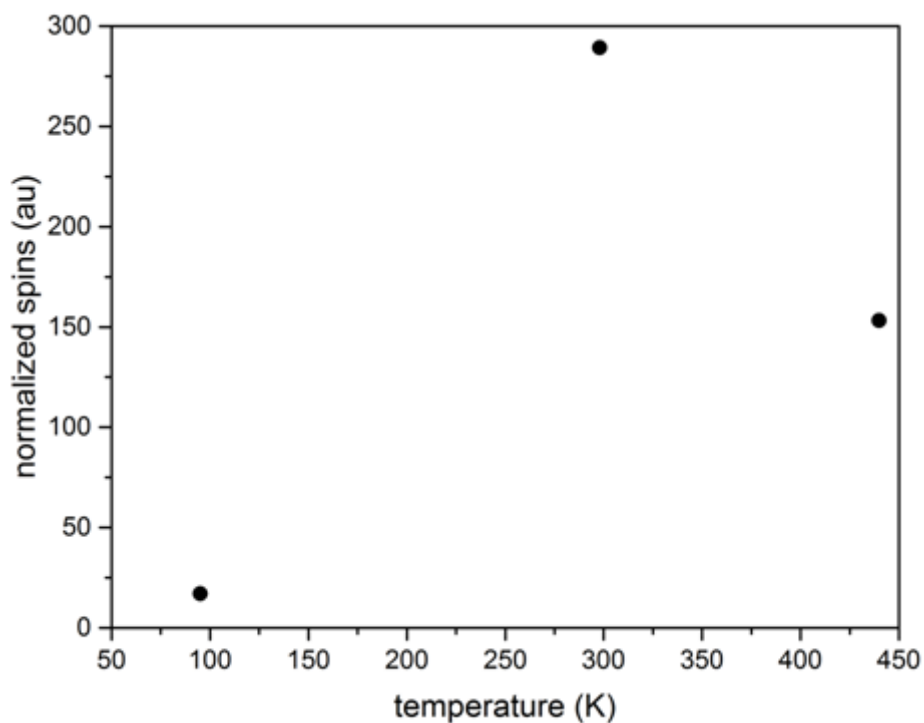4.4.4.2 Spin behavior of steam aged sample "CHA P 2.2 S"

Figure 4.14. Spin dependence on temperature for 2.2 % elemental copper weight sample "CHA P 2.2 S". Y axis is the double integration area of derivative ESR spectrum divided by resonator Q factor for normalization. Refer table B in appendix for details.

The total spins for steam aged sample, normalized for Q factor, when plotted against temperature of measurement yield non linearity as shown in figure 4.14. The ratio of intensity of steam treated sample measured at ~95 K to room temperature is 0.059 after normalization. This is the total integrated intensity after doing double integration of the derivative spectrum wherein the loss of intensity is compensated by improved spectral resolution. Another reason for such low intensity is the reduced modulation amplitude used for low temperature measurement as an effort to improve spectral resolution of hyperfine features. The highest spins were observed for sample measured at room temperature and then the spins decreased at ~440 K measurement. This highlights an approximate Curie paramagnetic spin behavior post hydrothermal aging for copper center precipitated in the zeolitic framework [26 and 36].

These spin transitions are due to deviation from Curie temperature behavior of Cu^{2+} spins in the external magnetic field at different temperatures. To know more about these variations a multi-step temperature variation analysis is required. We therefore plotted the dependence of spins with respect to temperature in figures 4.13 and 4.14 as initial analysis. The normalized spectral intensity for spectrum recorded at ~95 K was used for this comparative analysis. The non linear dependence of integrated intensity on temperature is an interesting trend for steam aged samples. Further analysis is required to describe spin transitions and catalytic phase deactivation of Cu^{2+} state at intermediate temperatures. In addition, cyclic temperature dependent studies are proposed to understand the changes that influence the Cu^{2+} ground state. Such trends

have been reported in the literature previously for lower temperature range up to room temperature [42, 43 and 44]. Additionally, phase separation analysis utilizing different power levels in ESR can help know more about spin behavior in these samples. These are proposed as future directives for these types of samples.

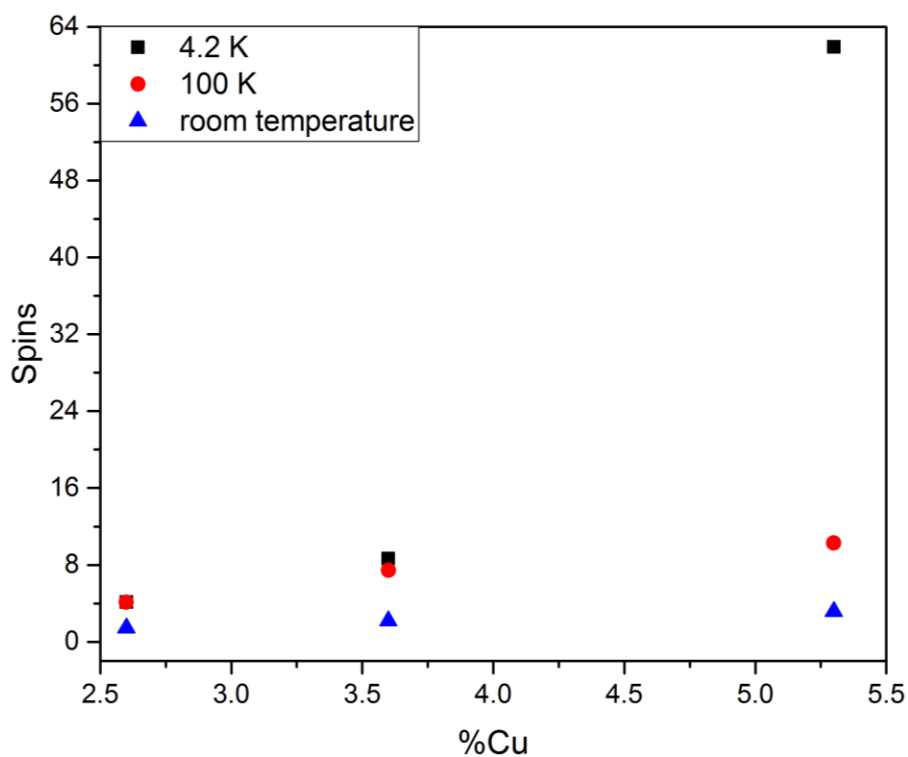**4.5 Quantitation of spins for increasing copper loading in ion exchanged samples**

Figure 4.15. Spins quantitation for samples with increasing copper loading in ion exchanged samples – FAU IE 2.6, FAU IE 3.6 and FAU IE 5.3. Y axis is the double integration area of derivative ESR spectrum divided by the product of Q factor and copper weight in milligrams in the sample for normalization. Refer Table B in appendix for details.

After the series of ESR investigations with many samples showing variation in copper center based on some isolable variables, it was necessary to do a spin quantitative analysis on increasing copper loading samples. A thorough gravimetric spin quantitative analysis is required for such an understanding of increasing copper loading. The results of such an analysis are reported in figure 4.15 and the standardization method is detailed in appendix A. In this gravimetric analysis, performed as weight by difference approach, sample weight was calculated by subtracting weight of empty tube from weight of sample containing ESR tube. Then based on sample weight and the percentage of copper content in the sample we calculate the weight of copper taken in the sample in ESR tube. Such weights were used to normalize signal amplitude ie second integration of derivative ESR spectrum was divided by the weight of copper to get the y axis. The x axis is the ICP AES measured percentage copper weight. The y axis is a reflection of ESR active copper in +2 oxidation state. The sample weight details and ESR parameters are given in appendix A and appendix B, respectively. Overall, we see a linear trend of increasing spins with increasing copper loading in figure 4.15, for axial copper centers with 2.6 and 3.6 % Cu wt at all temperatures. Interestingly, almost all of the copper is detected at ~100 K for copper concentrations of 2.6 and 3.6 % Cu wt, with the 2.6% Cu wt showing no benefit of measurement at ~4.2 K for the amount of samples taken in ESR tube. This indicates that these centers are behaving as normal copper (II) centers achieving ground state of +2 oxidation state by ligand stabilization [46]. A similar trend is observed for the sample with 5.3% Cu wt but it deviates at low temperature of ~4.2 K by transitioning to full non axial copper center with change in

geometry. Hence, it appears a case of saturation of preferred copper sites at concentrations in the range of 3.6 - 5.3 % Cu wt.

It was assumed that these samples were measured in a non saturation regime for the power level used. Power saturation studies can be done using a Curie plot analysis. An example of power saturation analysis would involve signal amplitude (double integrated intensity of derivative signal) versus the square root of microwave power (varied in 10 dB attenuation steps). Such studies can be simulated using a suitable spin Hamiltonian model. A thorough power saturation study would have to be carried out at each temperature level for each sample varied across the available power levels to understand the temperature dependent spin states better. Partial excitation of multiple species, if present, is expected in such an analysis. Such an analysis is proposed under the future scope for research on these samples.

5. Conclusions and future scope

This research has shed a new light on copper doped zeolites as NH_3 SCR catalysts. Several intrinsic & extrinsic chemical properties for the copper center in +2 oxidation state are understood. We can establish based on $g_∥$ and associated hyperfine splitting factor that the spin associated with the unpaired electron is delocalized in $d_{x^2-y^2}$ subset of d^9 orbital Cu^{2+} center [30 and 32-36]. It can be concluded that the resultant g factor interactions between local Cu^{2+} ion microenvironment and the whole crystal lattice is of spin lattice type for non diluted magnetic dipole interaction of separate Cu^{2+} ion in these systems [46]. The reported g factors are all axial ($g_z = g_∥$, $g_x = g_y = g_⊥$) with $g_∥ > g_⊥ > g_e = 2.0023$ [32]. This common situation corresponds to the case for Cu^{2+} in approximate square planar or tetragonally elongated octahedral coordination (approaching or deviating from D_{4h} local site symmetry). The highest occupied orbital has one unpaired electron, spin S = $^1/_2$, and corresponds to $d_{x^2-y^2}$. This orbital is directed in space towards four ligands that produce roughly the same electron repulsion but stronger compared to the ligand pair on the tetragonal axis (for the octahedral case). These g factors eliminate lower site symmetries such as five-coordinate ligand fields of square pyramidal or trigonal bipyramidal geometry or three-coordinate trigonal geometry. This Cu^{2+} center exhibits a distorted square planar geometry deviating from D_{4h} to D_{2d} symmetry [47]. A d^9 copper center also shows strong Jahn Teller effect, which leads to elongation or contraction along one of the coordinate axis, commonly assigned as z axis. This Jahn Teller effect helps minimize the free energy by increasing the energy splitting

of d orbitals to allow stability of +2 oxidation state in copper. The value of $g_\perp = 2.09 > g_e$ is small compared to some square planar complexes and thus may indicate the ligand field corresponds more closely to that of six coordinate tetragonal complexes [32-35 and 47]. The value of the ^{63}Cu magnetic hyperfine splitting was partially resolved on the $g_\parallel$ tensor ($A_\parallel$) but not on $g_\perp$ ($A_\perp$). The deviation from planarity is considered essential to achieve fast ligand exchanges, bond cleavage of N-O, bond formation of N-N and O-H bond via rapid redox transformation at the copper center from +2 to +1 oxidation state and then back to +2 oxidation state [41, 42 and 46]. Such a molecular understanding of copper in +2 oxidation state can help understand the mechanism of these catalysts better.

Our studies at ~4.2 K did not show any superhyperfine structure. Such absence of superhyperfine structure is expected in oxide lattices of zeolite type. This proves consistency in the copper core of a specific geometry and spatial coordination throughout the various treatments that were applied to deduce the ground state of copper. We also know that the copper center prefers specific coordination site in the zeolite framework based on several spin dependent ESR analysis reported here and tries to occupy that site through mobility in irregular doping. Such interactions are temperature dependent and it can be seen from above graphs the effect of temperature variation changes the spectra. In addition, adsorbed water versus bound water as part of coordination complex forms another parameter for interactions of copper centers. The copper center g factors of ion exchanged samples show approximate isotropy at

room temperature and at lower temperatures, they show anisotropy. For the calcined samples at room temperature, rhombicity is seen in the precipitated type whereas the ion exchanged sample shows axial geometry. At lower temperatures, both calcined samples show axial geometry. For the calcined sample of chabazite type of zeolite, the copper centers have undergone unequal transitions leading to speciation. A hydrothermal aging experiment gave some further insights on these copper centers in catalysts suggesting that water plays an important role as a ligand to allow stabilization of formal +2 oxidation state. Such hydrothermally treated samples show the merging of two species into one at room temperature and at higher temperature with approximate g factor isotropy.

These new insights about copper doped zeolites can help the better design of these highly selective functional catalysts. Future studies directed towards absorption studies such as energy absorption and UV Vis type to understand the molecular energy picture further are planned. A thorough study of temperature dependent spin behavior is also necessary to determine the nature of copper in the large temperature change window of diesel engine operation. Such studies will further optimize the design of these state of the art catalysts.

To conclude, the copper doped zeolite catalysts have specific variations based on the local environment of copper centers, which permit the rapid redox reactions via change of one oxidation number to achieve the highly selective NH_3 SCR catalysis.

References

[1] Frank J De Rewal, US Patent US2 030 283 A, February 11, 1936

[2] Leonard H Garey, US Patent US2 540 663 A, February 6, 1951

[3] Steam: Its Generation and Uses, Babcock and Wilcox Corporation

[4] Donald H Rosback, US Patent US3 649 177 A, March 14, 1972

[5] Dallas T Pence and Thomas R Thomas, US Patent US4 220 632 A, September 2, 1980

[6] John R Gladden, US Patent US4 188 364 A, February 12, 1980

[7] Garbis H Meguerian and Yasuo Kaneko, US Patent US3 953 576 A, April 27, 1976

[8] George L Bauerle, S C Wu and Ken Nobe, Parametric and Durability Studies on NOx Reduction with NH3 on Fe-Cr Oxide Catalysts, Ind Eng Chem Prod Res Dev, 1978, 17, 2, 123–128

[9] Kazuhide Miyazaki and Kiyomi Abe, US Patent US3 979 337 A, September 7, 1976

[10] John Smith Zink and Hershel E Goodnight, US Patent US4 004 875 A, January 25, 1977

[11] Pure & Appl Chem, 1994, 66, 8, 1739-1758

[12] https://engineering.purdue.edu/~thomsonk/image/ZSM-5.jpg

[13] http://www.mindat.org/min-35126.html

[14] Carmela Aprile, Avelino Corma and Hermenegildo Garcia, Enhancement of the photocatalytic activity of TiO2 through spatial structuring and particle size control: from subnanometric to submillimetric length scale, Physical Chemistry Chemical Physics, 2008, 10, 769–783

[15] Ch Baerlocher, LB McCusker and DH Olson, Atlas of Zeolite framework Types, Elsevier, Amsterdam, 6th ed, 2007

[16] http://www.iza-structure.org/databases/

[17] I Bull, RS Boorse, WM Jaglowski, GS Koermer, A Moini, JA Patchett, WM Xue, P Burk, JC Dettling and MT Caudle, US Patent US0 226 545, 2008

[18] Trong D Pham, Matthew R Hudson, Craig M Brown and Raul F Lobo, Understanding Carbon Dioxide Adsorption On Alkali Metal Exchanged Zeolite SSZ-13, Conference proceedings - separations division, 2013 Annual meeting, American Institute of Chemical Engineers

[19] http://webmineral.com/data/Mordenite.shtml

[20] http://www.wako-chem.co.jp/english/labchem/product/analytical/HSZ/images/M.gif

[21] Roald Brosius and Johan A Martens, Reaction mechanisms of lean-burn hydrocarbon SCR over zeolite catalysts, Topics in Catalysis, 2004, 28, 1, 119-130

[22] Sandro Brandenberger, Oliver Kröcher, Arno Tissler and Roderik Althoff, The State of the art in Selective Catalytic Reduction of NOx by Ammonia Using Metal Exchanged Zeolite Catalysts, Catalysis Reviews, 2008, 50, 4, 492-531

[23] Antonio Grossale, Isabella Nova, Enrico Tronconi, Daniel Chatterjee and Michel Weibel, NH_3–NO/NO_2 SCR for Diesel Exhausts After treatment: Reactivity,

Mechanism and Kinetic Modeling of Commercial Fe- and Cu-Promoted Zeolite Catalysts, Top Catal, 2009, 52, 1837–1841

[24] Lei Ma, Yisun Cheng, Giovanni Cavataio, Robert W McCabe, Lixin Fu and Junhua Li, Characterization of commercial Cu-SSZ-13 and Cu-SAPO-34 catalysts with hydrothermal treatment for NH3-SCR of NOx in diesel exhaust, Chemical Engineering Journal, 2013, 225, 323–330

[25] IUPAC, Compendium of Chemical Terminology, 2nd edition (the "Gold Book"), Compiled by A D McNaught and A Wilkinson, Blackwell Scientific Publications, Oxford, 1997

[26] RS Drago, Physical methods in Chemistry, W B Saunders company, Philadelphia, 1977, 316-351

[27] http://hyperphysics.phy-astr.gsu.edu/hbase/molecule/imgmol/esr1.gif

[28] CP Poole, Electron Spin Resonance, Wiley Interscience Publishers, 2nd edition, 1967

[29] N J Bunce, "Introduction to the interpretation of electron spin resonance spectra of organic radicals.", J Chem Educ, 1987, 64, 11, 907

[30] Eduardo Di Mauro and Walter Sano, Hyperfine and superhyperfine interactions in the ESR perpendicular spectra of Cu^{2+} in NH_4Br (acidic), Journal of the Physical Society of Japan, 1994, 63, 6, 2078-2081

[31] Maria-Teresa Turke, Igor Tkach, Marcel Reese, Peter Hoferb and Marina Bennati, Phys Chem Chem Phys, 2010, 12, 5893–5901

[32] Garriba E and Micera G, J Chem Educ, 2006, 83, 1229

[33] Moore R, Di Magno S and Yoon H W, J Chem Educ 1986, 63, 818

[34] Butera R A and Waldeck D H, J Chem Educ, 2000, 77, 1489

[35] Basu P, J Chem Educ, 2001, 78, 666

[36] Wertz J E and Bolton J R, Electron Spin Resonance: Elementary Theory and Practical Applications, Chapman and Hall, New York, 1986

[37] Kon et al, Pure & Appl Chem, 1989, 61, 12, 2195-2200

[38] János Inczédy, Tamás Lengyel, Allan M Ure, András Gelencsér, Adam Hulanicki, Compendium of Analytical Nomenclature, Definitive Rules, International Union of Pure and Applied Chemistry, 1997, 3rd edition, Chapter 14.2

[39] http://web.uvic.ca/~berryde/commonfiles/appendix2.pdf

[40] Chundi Yan, Hao Cheng, Zhongshan Yuan and Shudong Wang, The role of isolated Cu^{2+} location in structural stability of Cu-modified SAPO-34 in NH3-SCR of NO, Environmental Technology, 2015, 36, 2, 169-177

[41] Anita Godiksen, Frederik N Stappen, Peter N R Vennestrøm, Fillipo Giordanino, Søren Birk Rasmussen, Lars F Lundegaard and Susanne Mossin, Coordination Environment of Copper Sites in Cu CHA Zeolite Investigated by Electron Spin Resonance, Journal of Physical Chemistry C, 2014, 118, 23126-23138

[42] Charles HF Peden, Ja Hun Kwak, Sarah D Burton, Russell G Tonkyn, Do Heui Kim, Jong-Hwan Lee, Hung-Wen Jen, Giovanni Cavataio, Yisun Cheng and Christine K Lambert, Possible origin of improved high temperature performance of hydrothermally aged Cu/beta zeolite catalysts, Catalysis Today, 2012, 184, 1, 245-251

[43] Junjie Xue, Xinquan Wang, Gongshin Qi, Jun Wang, Meiqing Shen and Wei Li, Characterization of copper species over Cu/SAPO-34 in selective catalytic reduction of NOx with ammonia: Relationships between active Cu sites and de-NOx performance at low temperature, Journal of Catalysis, 2013, 297, 56-64

[44] Feng Gao, Eric D Walter, Nancy M Washton, János Szanyi, and Charles HF Peden, Synthesis and Evaluation of Cu-SAPO-34 Catalysts for Ammonia Selective Catalytic Reduction. 1. Aqueous Solution Ion Exchange, ACS Catalysis, 2013, 3, 9, 2083–2093

[45] IM Procter, BJ Hathaway and P Nicholls, J Chem Soc (A), 1968, 1678

[46] OJ Ballhausen, "Introduction to Ligand Field Theory", McGraw-Hill, New York, NY, 1962, 108 and 185

[47] H Yokoi and AW Addison, Inorganic Chemistry, 1977, 16, 6, 1341-1349

Appendices

A. Quantitation standardization

Copper content in +2 oxidation state was quantified by preparing a standard of known copper concentration as a control. The most common standard for these studies can be prepared by using copper sulfate salt dissolved in a common glassing solvent. Four concentration standards of 0.5, 1, 1.5 and 2 mM concentration were prepared using 25 mg of $CuSO_4 \cdot 5H2O$ dissolved in 50 ml of 25% glycerol solution both from commercial sources. These gave $[Cu (H_2O)_6]^{2+}$ which served as a model Cu^{2+} center. The standards were prepared in low concentrations to keep the Cu^{2+} centers as monomeric as possible without any interference to get a well resolved ESR spectrum, as shown in figure A1, which could be pre-determined with theory.
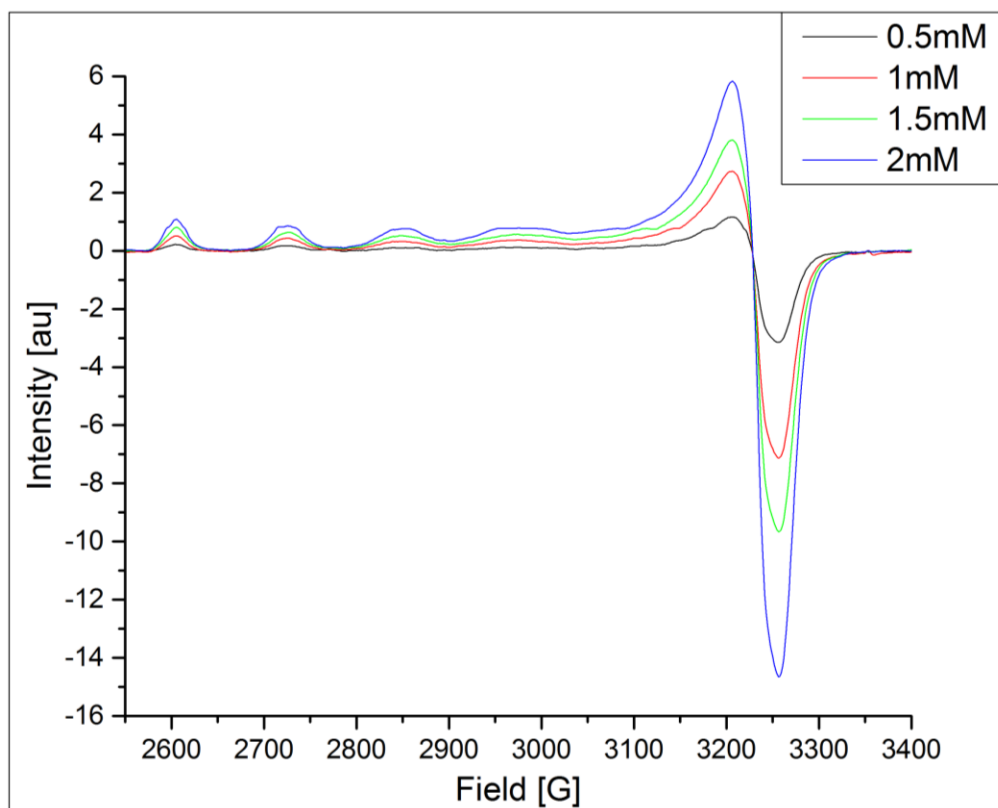
Figure A1. CW 1D field sweep ESR spectrum of concentration standards shows consistent hyperfine features as found in other samples under study. These spectra are measured at ~100 K.

The copper (II) content of these standards is analyzed using double integration of the original ESR signal by eliminating baseline from the spectrum. The area under the absorption curve gives us a value that is in direct relation with the copper (II) content. It should be recalled here that the ESR spectrum is generally in derivative mode.

The following table A will serve as a guide for quantitation analysis of concentration standards.

Table A. Analysis of the amount of copper taken for ESR measurements.

Sample	ESR tube wt, g ($\pm$0.001 g)	ESR tube + sample wt, g ($\pm$0.001 g)	Sample wt, mg ($\pm$1 mg)	Calculated Copper wt in sample, mg
2.6% Cu	3.473	3.817	344	8.9
3.6% Cu	3.102	3.384	282	10
5.3% Cu	3.567	3.92	353	19
0.5 mM	3.448	4.155	707	0.084
1 mM	3.019	3.825	806	0.19
1.5 mM	2.792	3.562	770	0.273
2 mM	2.658	3.442	784	0.370

Note that the concentration standards prepared here are of far lesser concentration than the samples provided for analysis. Still, the spin relation of concentration standards with copper content is linear as shown in figure A2.
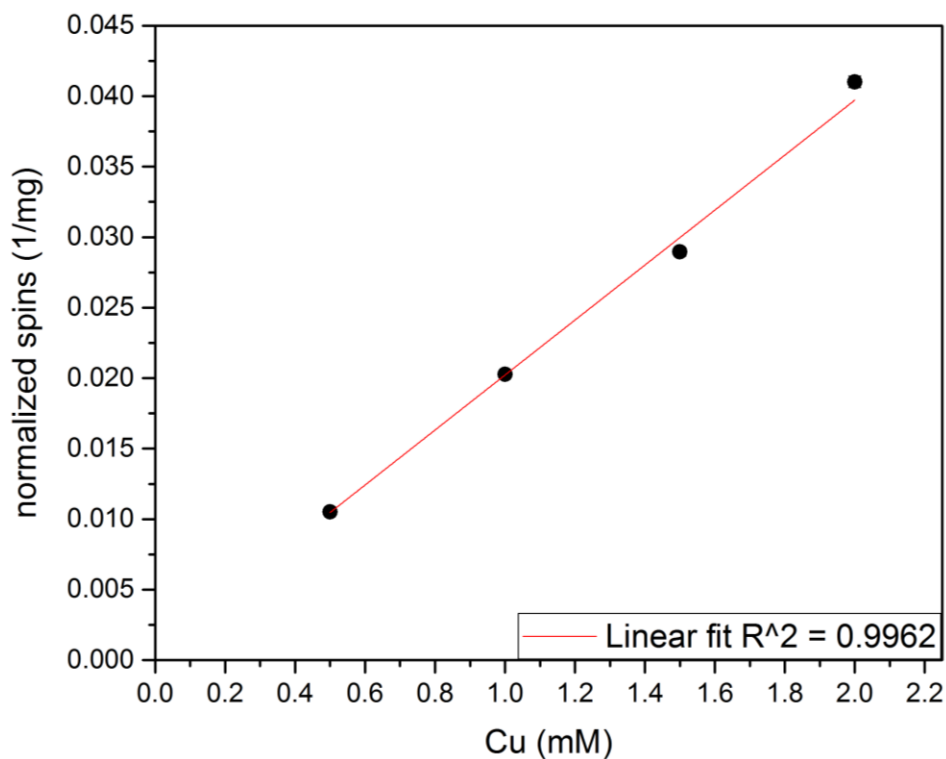
Figure A2. Quantitation of copper content in concentration standards of 0.5, 1, 1.5 and 2 mM concentration using double integration of ESR derivative spectrum. The normalized spins on y axis are calculated by taking the second integral area of derivative ESR spectrum and dividing such integrated area by the product of the amount of sample weight in milligrams and the resonator Q factor.

When this quantitation of concentration standards is simulated in the region of copper concentration of unknown samples, we still observe a linear relationship of spins with increasing copper content as shown in figure A3.
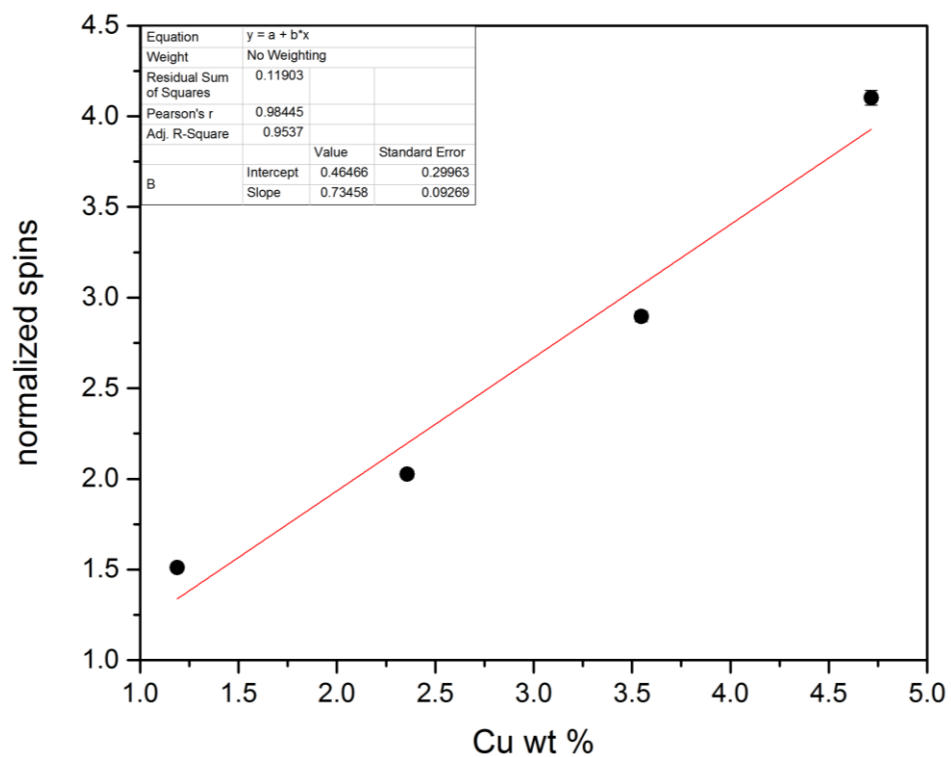
Figure A3. Extrapolation of copper content quantitation of concentration standards in the region of Copper weight percentage of unknown samples. The spin normalization is same as that described in figure A2.

This standardization helps in establishing spins in the unknown by comparing spectral features and the number of spins.

B. Spectral analysis

Several important parameters deduced from the raw ESR spectra are detailed below with respect to sample ID.

Table B. Sample g factors, hyperfine splitting values and peak to peak width.

Sample ID	Temperature K (± 1 K)	$g_\parallel$ (± 0.001)	$g_\perp$ (± 0.001)	$a_\parallel$, G (± 3 G)	ΔH_{pp}, G (± 3 G)	Q factor	Gain dB	Power mW	Frequency GHz	MA G
FAU IE 2.6	~4.2	2.392	2.092	139	75	3400	30	10.08	9.482	4
FAU IE 3.6		2.386	2.094	144	84	3600	30	10.08	9.483	4
FAU IE 5.3		2.392	2.055	139 $a_\perp = 48$ G	127	3800	30	10.11	9.483	4
FAU P ~2.4 C		2.406	2.087	129	82	7800	30	0.2012	9.693	1
FAU IE 2.67 C		2.402	2.087	133	94	7800	30	0.2012	9.696	1
CHA P 2.2 C	~95 K	2.39	2.09	140	~100	3800	70	0.6362	9.426	4
CHA P 2.2 S		2.39	2.10	136	~100	3500	55	0.6362	9.429	4

MA = Modulation Amplitude

ESR Parameters

FAU IE 2.6, FAU IE 3.6 & FAU IE 5.6:	**FAU IE 2.67 C and FAU P 2.4 C:**	**CHA P 2.2 C and CHA P 2.2 S:**
Figure 4.3	Figure 4.6 and figure 4.9 respectively	Figure 4.12
Modulation Frequency = 100 kHz	Modulation Frequency = 100 kHz	Modulation Frequency = 100 kHz
Number of scans = 3	Number of scans = 5	Number of scans = 2
Conversion time = 81.92 ms	Conversion time = 40.96 ms	Conversion time = 81.92 ms
Sweep time = 335.54 s	Sweep time = 41.94 s	Sweep time = 335.54 s
Time constant = 327.68 ms	Time constant = 40.96	Time constant = 327.68 ms
Resonator = ER 4102 ST	Resonator = ER 4118 CF	Resonator = ER 4102 ST
Resolution = 4096	Resolution = 1024	Resolution = 4096